X-29A Aircraft Structural Loads Flight Testing

Robert Sims, Paul McCrosson, Robert Ryan, and Joe Rivera

NASA

X-29A Aircraft Structural Loads Flight Testing

Robert Sims
NASA Ames Research Center, Dryden Flight Research Facility, Edwards, California

and

Paul McCrosson, Robert Ryan, and Joe Rivera
Grumman Aircraft Systems, Grumman Aerospace Corporation, Edwards, California

X-29A AIRCRAFT STRUCTURAL LOADS FLIGHT TESTING

Robert Sims*
NASA Ames Research Center
Dryden Flight Research Facility
Edwards, California

and

Paul McCrosson,[t] Robert Ryan,[t] and Joe Rivera[t]
Grumman Aircraft Systems
Grumman Aerospace Corporation
Edwards, California

Abstract

The X-29A research and technology demonstrator aircraft has completed a highly successful multiphase flight test program. The primary research objective was to safely explore, evaluate, and validate a number of aerodynamic, structural, and flight control technologies, all highly integrated into the vehicle design. Most of these advanced technologies, particularly the forward-swept-wing planform, had a major impact on the structural design.

Throughout the flight test program, structural loads clearance was an ongoing activity to provide a safe maneuvering envelope sufficient to accomplish the research objectives. This paper presents an overview of the technologies, flight test approach, key results, and lessons learned from the structural flight loads perspective. The overall design methodology was considered validated, but a number of structural load characteristics were either not adequately predicted or totally unanticipated prior to flight test. While conventional flight testing techniques were adequate to insure flight safety, advanced analysis tools played a key role in understanding some of the structural load characteristics, and in maximizing flight test productivity.

Nomenclature

ACC	automatic camber control
AR	analog reversion
c.g.	center of gravity
FCS	flight control system
FOL	flight operating limit
h	pressure altitude, ft
ITB	integrated test block
KEAS	knots equivalent airspeed

M	Mach number
MAC	mean aerodynamic chord, in.
MCC	manual camber control
Mil-Spec	military specifications
N_Z	load factor, corrected to design weight, g
ND	normal digital
$\bar{q}$	dynamic pressure, lb/ft^2
WS	wing station, in.
α	angle of attack, deg
β	angle of sideslip, deg
δ_C	canard position, deg
δ_F	wing flaperon position, deg

Introduction

The advent of aeroelastic tailoring with composite materials made the practical application of a forward-swept wing to a high performance vehicle a viable design concept. While offering potential performance benefits, the forward-swept-wing planform is inherently divergence prone. Validation of this technology through the reality of flight test was obviously required, which led to the design and development of the X-29A aircraft. As the design evolved, a number of other advanced technologies were incorporated, such as the close-coupled canards and high degree of static instability. These technologies are described in detail in a following section. The evolution, design, and development of the X-29A aircraft is documented in Refs. 1–3.

Following extensive ground testing, the flight test program was initiated in December 1984 at the Dryden Flight Research Facility of the NASA Ames Research Center. The basic envelope expansion and follow-on research phases spanned approximately four years and were conducted by a joint test team made up of NASA, Air Force Flight Test Center, and Grumman Aerospace Corporation personnel. Initial envelope expansion was accomplished in a cautious,

*Lead structures flight test engineer, X-29A Program.
[t]Structures flight test engineer, X-29A Program.
[t]Lead Grumman flight test engineer, X-29A Program.

buildup fashion addressing the concerns of control system stability, flutter, aeroservoelasticity, stability and control, flying qualities, propulsion, and structures. The research phase acquired more detailed data, primarily in the areas of performance, pressure distributions, divergence, buffet, parameter identification, handling qualities, military utility, and agility. The flight control system software also underwent several updates including modified control surface schedules and increased agility control laws. To support these activities, structural loads maneuver clearance was required throughout the flight program. A program overview, flight test techniques, and results in the other disciplinary areas are documented in Refs. 4–16 and for structural dynamics (Kehoe, Michael W. and Rivera, Joseph A., NASA Technical Memorandum, to be published). The subject of wing divergence flight testing, while intimately related to structural loads, has been previously reported in Ref. 17, and will not be addressed in this paper.

This paper presents an overview of the flight test program from the structural flight loads perspective. Background material includes a description of the advanced technologies, the vehicle design, and the structural measurements. The flight test approach is addressed in detail including the test phases and objectives, maneuvers and test matrices, real-time monitoring, postflight processing, database management, and load prediction capability. Key results illustrate general loading trends for the wing, canard, and flaperons relative to flight limits and predictions. Emphasis is placed on loading characteristics possibly unique to the X-29A design and its technologies, many of which were not anticipated prior to flight test. Characteristics that were dependent on the control law implementation and its revisions are also highlighted. The paper closes with a summary of the major accomplishments, key findings, lessons learned, and some general observations resulting from the flight test of this unique aircraft.

Aircraft Description

A photograph of the X-29A aircraft is shown in Fig. 1 with the physical characteristics of the design illustrated in Fig. 2. The aircraft size approximates that of the Northrop F-5 airplane, placing it in the lightweight fighter category. An F-404-GE-400 engine, as used in the F-18 aircraft, provides 16,000 lb of thrust. The side-mounted engine inlets are a simple, fixed configuration optimized for the transonic region. Total fuel capacity is 4,000 lb contained in four tanks located in the fuselage and aft wing strakes. The wing itself is dry, with no provision for aerial refueling. The wing design incorporates hard points, but no external stores are carried. The main landing gear is adapted from the F-16 design. An inlet for the environmental control system is contained in the large fairing at the base of the conventional vertical stabilizer and rudder.

A total of nine integrated servoactuators power the control surfaces: two canards, four wing flaperons, two strake flaps, and the rudder. Canard and strake flap surfaces op-erate symmetrically only, with roll control coming from the flaperons alone. The outboard and mid flaperons are tied to a common actuator located in a pontoon fairing mounted to the lower wing surface because of the thin airfoil cross section. Actuators buried in the wing root are connected to the inboard flaperons with pushrods. Inboard and outboard actuators are geared such that all three flaperon segments move similar amounts for roll or pitch commands. Control surface throws are $+30/-60°$ for the canard, $+25/-10°$ for the flaperon, and $\pm30°$ for the strake flap and rudder. Maximum control surface rates are 105 deg/sec for the canard, 68 deg/sec for the flaperon, 27 deg/sec for the strake flap, and 141 deg/sec for the rudder. With the exception of the strake flaps, all actuators are of modified F-16 design. The dual hydraulic system is a conventional 3,000 lb/in.^{2} design adopted from the F-14 aircraft.

The flight control system (FCS) incorporates two primary flight modes: normal digital (ND), and analog reversion (AR) for backup. Flight control system gains are extensively scheduled with flight condition. The flight control computers utilize triplex digital channels operating at 40 Hz. Triplex analog channels use separate and redundant sensors. The analog backup mode incorporates many simplifications and was thus considered a "get home" mode not designed for aggressive maneuvering. The standard flight mode is ND with automatic control surface scheduling. These schedules, called automatic camber control (ACC), adjust the canard, wing flaperons, and strake flap as a function of flight condition to provide optimum aerodynamic efficiency (lift-to-drag ratio) throughout the flight envelope. In addition to ACC, a fixed wing flap manual camber control (MCC) mode was incorporated for research purposes. In this mode, the canard and strake flap do whatever is necessary to trim the aircraft while the wing flap remains at a fixed position. Pilot selectable in 5° increments, this mode was invaluable and highly utilized in the gathering of data for pressure distribution, buffet, performance, divergence, and loads research because it maintained a fixed wing geometry throughout a maneuver. On the debit side, it was an additional mode that had to be cleared. It is also worth noting that maneuvers employing the MCC mode and the AR mode were not included in the original structural analysis of the airplane. More detailed descriptions of the X-29A design and the FCS implementation are found in Refs. 3 and 12.

Technology Description

The advanced technologies integrated into the X-29A design include the forward-swept wing with aeroelastically tailored composite covers, a thin supercritical wing airfoil, three-surface pitch control, double-hinged wing flaperons, full-authority close-coupled canards, aft-mounted strake flaps, and high static instability. A digital fly-by-wire control system is necessary to make all the advanced technologies work together. These technologies will be described in some detail including, where relevant, a discussion of their structural implications.

2

The forward-swept-wing planform is a very prominent feature, with a structural axis (mid box) sweep angle of $-36.2°$. The inherent divergence tendencies of this configuration are controlled through the use of aeroelastically tailored composite wing skins, with an insignificant weight penalty over that required for the basic strength design. With proper ply orientation, bend-twist coupling combined with high material stiffness properties minimizes the natural wash-in tendencies under load. Even so, the aeroelastic properties remain significantly adverse. For example, the wing lift coefficient due to angle of attack had a predicted elastic-to-rigid ratio of about 1.6 at the design dynamic pressure (1,700 lb/ft^2 at Mach 1.07 and sea level altitude). Conventional aft-swept wings have elastic-to-rigid ratios less than 1. Errors in the predicted load distributions or stiffness characteristics could lead to greater load amplifications and a lower divergence boundary for a forward-swept-wing design. This technology obviously required a great deal of attention throughout the analysis, design, ground test, and flight test phases.

The wing planform has substantial built-in twist with no leading-edge devices. The thin supercritical airfoil is of third-generation design with a thickness-to-chord ratio varying from 5 to 7 percent. Three-surface pitch control is achieved through the simultaneous movement of the canard, full-span wing flaperons, and the aft strake flaps. The wing flaperons are dual hinged at the 75 and 90 percent chord. The "tab" surface is geared 2 to 1 relative to the main panel which results in a powerful, efficient control surface for both roll and pitch. The concept is referred to as "discrete variable camber" and is considered to be a low-cost alternative to smooth variable camber. The full-authority all-moving canard surfaces are truly close coupled to provide mutual interference with the wing aerodynamics. Canard area is relatively large — 20 percent of the wing reference area. As can be seen in the front view of Fig. 2, the canard has no dihedral and is coplanar to the wing surface. Canard downwash has a strong influence on the inboard wing loading. Likewise, wing upwash has a strong influence on the canard lift. Typically, canard lift due to angle of attack is approximately 1.5 times that due to canard incidence. Any misprediction of these interference effects could have a large influence on the load distributions of both surfaces.

To a great degree, the extremely high levels of static airframe instability are simultaneously created and controlled by the fore-mounted canards. Static margin is -35 percent subsonically, with the airframe becoming neutrally stable at supersonic speeds. Without the canards, the airframe is neutrally stable at subsonic speeds. This level of instability is made possible by the full-time, digital fly-by-wire flight control system. If the FCS suffered a total failure, the predicted time to double amplitude is approximately 140 msec at transonic, low-altitude conditions. Fortunately, this level of instability has never been demonstrated in flight, because of the virtually flawless performance of the FCS. The structural implications for control surfaces responding to this instability level were largely unknown prior to flight test.

Techniques for implementing the ACC control surface schedules for a three-surface, highly unstable aircraft are not obvious and deserve a more detailed explanation because they affect the way the aircraft trims. In the X-29A design, the pitch stabilization task is handled by a fast-rate inner control loop that is separate from the slower acting outer loop that controls the ACC function. The control surface schedules are implemented as tables of optimum canard position as a function of angle of attack, and strake flap position as a function of flaperon position. Each table is a function of Mach number and altitude. The wing flaperons are commanded to whatever position is necessary to keep the mean canard position near optimum. If the flaperons reach their full down position, the strake flap is positioned such that optimum canard position is maintained. The canard is thus the priority surface in the optimization scheme. The ACC function must operate at a relatively slow rate to not interfere with the primary pitch stabilization task. The impact of the slow-acting ACC function during an abrupt pitch maneuver will be discussed in the results section. The highly augmented FCS dominates the aircraft response and controls maneuver authority as a function of flight condition. The FCS design provides some degree of structural loads protection, as long as the FCS operates as expected and the load distributions are predicted correctly. The critical design loads are thus intimately tied to the FCS as it existed during the design phase, and any FCS updates that change the general maneuvering characteristics need to be evaluated relative to their impact on the structural loads.

Structural Design and Proof Test

With the exception of the wing, the X-29A structure was built using conventional materials and design concepts. The aeroelastic tailoring and stiffness requirements for the wing dictated the use of graphite-epoxy composite upper and lower covers bolted to a metallic substructure. Titanium was used for the main front spar and aluminum for the rear and four intermediate spars. The composite covers are continuous from wingtip to wingtip and are relatively thick (0.83 in. at the root region). A large number of plies of various orientations are utilized to optimize the bend-twist coupling and stiffness characteristics. Further details of the ply layups and other aspects of the composite design cannot be addressed in this paper because of data dissemination restrictions.

Standard Air Force military specifications (Mil-Specs) for external loads, fatigue, and damage tolerance were applied throughout the design. The methodology used for the external loads analysis will be described briefly in the section dealing with load prediction capability. Key structural design criteria included a maximum Mach number of 1.72 and a maximum dynamic pressure of 1,700 lb/ft^2. Design symmetric load factors were 8-g subsonic and 6.5-g supersonic for a maneuver gross weight of 15,000 lb. Asymmetric load factors were the standard 80 perccent of symmetric values. Design fatigue life was 3,000 hr.

3

Because the proof test and flight articles were one and the same, static testing was conducted to 100 percent of design limit and not ultimate load, which would be done for a production aircraft program. As a result, flight load factors were limited to 80 percent of design (6.4-g subsonic and 5.2-g supersonic). Structural limits were generally restricted to 80 percent of proof test values. Some notable exceptions to this philosophy were made during the flight program and are addressed in the results section. During the proof tests, the wing structure received considerable attention to verify both its strength and stiffness. Three separate 8-g design loadings were applied with generally good correlation with predictions. Measured deflections indicated that the wing was slightly more flexible than expected. Streamwise twist at the wingtip was 6 percent higher than predicted. Proof loads were also applied to the canard, fuselage, flaperon, strake flap, and vertical tail structures. The total proof test effort required the measurement of 470 strain gage channels, 103 deflection channels, and 45 hydraulic jack loads.

Structural Measurements

The primary structural measurements were derived from strain gages calibrated to measure shear, bending moment, and torsion at nine stations. There were four stations on the left wing, and one station each on the right wing root, left- and right-canard roots, the mid fuselage, and the vertical tail root. Load equations were developed using the conventional point load calibration technique of Ref. 18. From a total of 114 active strain gage channels, 71 were dedicated to the calibrated load equations. The remaining 43 channels were allocated to discrete strains, wing and flaperon link loads, and control surface actuator loads. The strain gage distribution by component was 55 for the wing, 12 for the flaperons, 6 for the strake, 21 for the canard, 9 for the fuselage, and 11 for the vertical tail. Note that approximately half of the measurements were devoted to the wing structure because of its new technology. The standard data sampling rate for the strain gage channels was 50 samples/sec. When substantial buffet loads were encountered, the sampling rate for 14 selected parameters was increased to either 200 or 400 samples/sec. Information describing the instrumentation system is contained in Ref. 7.

Details of the wing load measurement stations are shown in Fig. 3. The structural box transitions from unswept inboard to swept constant chord lines outboard. The load stations were oriented to place the torsion axes midway through the box. The four stations provided good coverage across the span, which was expected to have an unconventional span load distribution, particularly in the inboard region because of the strong canard downwash. The wing box cross section shows the typical strain gage installation at each station. Eighteen bridges were installed at each station, including some on the composite covers. Typically half of these were active channels which fed the shear, bending moment, and torsion equations. Some of the equations utilized gages installed on the composite. Equation accuracies were con-

sidered typical of NASA Dryden's experience with conventional all-metallic structures.

The canard load measurements are detailed in Fig. 4. With the torsion axis aligned with the spindle, this measurement is equivalent to a control surface hinge moment. Strain gages are tightly clustered around the spindle juncture as would be done for a conventional horizontal stabilizer. Note the relatively low aspect ratio for this surface. The mean aerodynamic chord is large relative to that of the wing (a ratio of 0.76). The location of the torsion axis is about midway between the 25 percent and 50 percent mean aerodynamic chord (MAC) points to balance the subsonic as opposed to supersonic hinge moments. This location represents a major tradeoff because the torsion axis is not conservatively located from a divergence viewpoint. In essence, the wing is not the only surface that is inherently divergence prone. Fortunately, the pitch-loop stiffness required for control system stability resulted in a predicted divergence boundary that was well beyond that for the wing. Canard surface free play was a major concern that was tracked throughout the flight program.

Flight Test Approach

Program Phases and Objectives

A chronology of the flight test phases and objectives is shown in Fig. 5. The limited envelope phase was conducted up to Mach 0.6 and 20° angle of attack. An update to the FCS software was required before expanding to higher Mach numbers. This update implemented additional variable gains to the AR backup mode. A modest amount of structural testing was accomplished within the limited envelope. A normal load factor of 5.3 g was demonstrated, as well as some abrupt maneuvering.

Following the FCS update, the program embarked on the major envelope expansion phase. As seen in the chronology, this phase lasted approximately one year, because of the cautious buildup approach required by all disciplines. Two integrated test blocks (ITB) were developed to satisfy the clearance requirements. The ITB-1 consisted of a stabilized point, control surface raps and doublets, and a pitch frequency sweep. This block expanded the 1-g airspeed and altitude envelope for control system stability, flutter, aeroservoelasticity, and stability and control. The ND, AR backup, and MCC modes had to be cleared with a separate ITB-1. The basic maneuvering envelope was cleared using ITB-2, which is described in more detail in the next section. Standard Mil-Spec structural maneuvers for abrupt and asymmetric maneuver clearance were not included in this phase. Throughout this complex expansion phase, the aircraft and its systems proved to be highly reliable, allowing multiple flights on a given day. However, even with sophisticated and comprehensive real-time monitoring, the long-term average fly rate of approximately two flights each week was governed by the time required for engineering analysis and flight planning.

After an extended layup for instrumentation upgrades, a follow-on research phase was begun. Initial emphasis was placed on acquiring detailed research data in the areas of performance, buffet, pressure distributions, parameter identification, and static wing divergence. This research required an extensive amount of windup turn symmetric load factor clearance in both the scheduled and fixed-flap modes. As seen in the Fig. 5 time line, abrupt and asymmetric maneuver clearance was not begun until well into the flight program. The objective was to clear an all-out maneuvering envelope sufficient to conduct a preliminary military utility and agility evaluation before implementing several planned FCS software updates.

These updates were staggered to allow sufficient time to clear and evaluate each update separately. With a substantial flight database to build on, testing of the two major updates was completed expeditiously, with less than 30 flights required to clear and evaluate each update. The first update incorporated revised ACC schedules and shortened longitudinal stick throws to improve control harmony. The revised ACC schedules were intended to improve the buffet characteristics and to reduce canard loadings in the transonic and supersonic high dynamic pressure region. This update required a reassessment and then a continuance of the loads clearance. The final FCS update that had an impact on the loads clearance was an increase in the pitch and roll agility. In the original control laws, pitch onset rates were intentionally constrained because of concern for the highly unstable airframe (the three-surface pitch control could perhaps generate more noseup moment than it could later arrest). The original roll rate authority was constrained to minimize potential roll-pitch coupling tendencies during the initial envelope expansion phase. The FCS update was designed to bring the X-29A agility characteristics more in line with contemporary fighters. Even after the update, additional control authority is available, but its impact on the FCS design and the original structural design constraints would have to be addressed. Again, this FCS update required another reassessment of the loads clearance. After completing the maneuver envelope clearance, a significant amount of agility work was completed, including some generalized air combat maneuvering. After 242 highly productive and safe flights, X-29A vehicle number 1 was placed in flyable storage. As with many flight programs, additional constructive flight testing could be conceived, but vehicle number 2 had already arrived at NASA Dryden to begin a dedicated high-angle-of-attack program.

Structural Maneuvers and Test Matrices

The structural flight test maneuvers were divided into two groups: the basic maneuvers block (ITB-2) and the extended maneuvers block. The basic maneuvers test block was generally conducted over the full envelope as required by the project objectives. Maneuvers included full-pedal steady sideslips, partial stick 0° to 60° rolls, full-stick 360° rolls, pushover-pullups from 0 g to 2 or 3 g, and slow onset windup turns. Sideslips and rolls were flown generally in the

ACC mode only. Pushover-pullups and symmetric windup turns were performed in both the ACC and MCC modes. In particular, static wing divergence clearance required fixed-flap maneuvers to extract load and deflection data as a function of angle of attack only. The basic maneuvers block laid the necessary foundation for the extended maneuvers block. This block addressed the standard Mil-Spec structural clearance maneuvers: abrupt pullups and pushovers, elevated g roll reversals, rudder kicks with abrupt release, and rudder reversals. These maneuvers, flown in the ACC mode only, cleared abrupt full-throw inputs for each of the three axes.

The test matrix completed for ACC windup turns is shown in Fig. 6. The normal load factor (N_Z) reached at each flight condition is identified. In this figure, and in all that follow, the load factor is referenced to the 15,000-lb design weight. The dense number of points does not represent the points required for structural clearance, but instead represents all points flown to satisfy the requirements of all disciplines. Typically, many research maneuvers are flown along constant dynamic pressure lines, instead of constant altitudes, as was done during the original envelope expansion. Initial load factor expansion was generally flown to the 4-g level for subsonic Mach numbers and the 3-g level for supersonic Mach numbers. Following postflight extrapolation of all load parameters, the load factor was cleared in several buildup steps up to the load factor, angle of attack, or buffet limit as dictated for each point. It should be emphasized that the primary structural objective was to provide adequate clearance to support the broad research priorities of all disciplines, and not to conduct a full envelope structural demonstration program as required for a production airplane. Thus, some points were not fully cleared to the limit load factor, particularly near the thrust-limited boundary. Nevertheless, the limit load factor was achieved at a number of subsonic, transonic, and supersonic conditions. Virtually the entire envelope below Mach 1 was recleared with the new ACC schedules.

An example test matrix for the MCC fixed-flap mode is shown in Fig. 7. The 0° position was the most utilized flap setting. Test conditions for the more positive (trailing-edge-down) positions greater than 5° were generally limited to the moderate 400 lb/ft² dynamic pressure range. The MCC mode was flown for research purposes only and no attempt was made to clear a broad, generalized envelope. Each combination of flap position and flight condition was cleared on a point-by-point basis for controls, flutter, and structural loads. In general, the aircraft trim and associated load distributions could be vastly different between the MCC and ACC modes. Even though the MCC mode was not considered in the original structural design, substantial load factors were achieved (up to 6.2 g), but the level of clearance was highly dependent on flap position and flight condition. Some combinations required definite restrictions which will be illustrated later.

The test matrix for abrupt symmetrical maneuvers is shown in Fig. 8. The priority envelope established for mil-

itary utility testing was bounded by Mach 0.95, 450 knots equivalent airspeed (KEAS), and 10,000-ft altitude. The military utility objectives required operating the X-29A aircraft between load factors of 6.4 g to -1 g. This envelope was considered barely adequate for the agility testing and air-to-air maneuvering. Limited test time and other project priorities necessitated a tradeoff between envelope size and the desire to evaluate the planned software updates. Some clearance was also worked below 10,000-ft altitude to support air-to-ground evaluations and potential airshow demonstrations. The envelope was expanded through an incremental buildup approach for both the original and increased pitch agility control laws.

The test matrix for asymmetric rolling maneuvers is shown in Fig. 9. With data from 1-g rolls and symmetric windup turns as a foundation, the elevated g roll reversals were cleared in steps to 3, 4, and 5 g using full lateral stick inputs. Partial stick buildup maneuvers were not required. The limit asymmetric load factor of 5.1 g was cleared for both the original and increased roll agility control laws.

The test matrix for directional maneuvers is shown in Fig. 10. With data from the steady sideslips as a foundation, abrupt rudder pedal kick and release maneuvers were performed. Good correlation with predictions for these maneuvers led to straightforward completion of the followup full-pedal reversal clearance. Because the vertical tail does not incorporate any new technologies, and the load levels reached within the military utility envelope were modest compared to structural limits, the vertical tail loads will not be addressed in the remainder of this paper.

Real-Time Monitoring

Throughout all program phases, real-time monitoring of all critical structural parameters was a standard part of the flight activity. Conventional displays included 4 strip charts (8 channels each), 24 annunciator lights, and a multipage video display containing flight condition and aircraft state data. In addition, an advanced color graphics unit was used to display strength envelopes for selected surfaces. Figure 11 shows three examples taken from a black and white hard copy unit. In Fig. 11(a), the data are from left- and right-roll reversals initiated at a symmetric load factor of 5 g. Starting from the upper left and moving clockwise, the display plots bending and torsion loads relative to strength envelopes for the canard, fuselage, outboard wing, and inboard wing stations. In general, the two sets of polygons represent the 80 and 100 percent design limits. Thus, the flight test maneuvers are flown with the objective being to stay within the inner boundary which represents the flight operating limit (FOL). As will be discussed in the results section, the limits for the canard surface were increased such that the outer polygon represents the flight-allowable values. Past data is saved in green and the current data point is displayed as a red dot. The digital data in the left column lists flight conditions, trim variables, and selected load parameters. The display can be frozen, dumped to hard copy, and reset between maneuvers. Alternate pages containing other load stations can be selected depending on the type of maneuver coming up next in the flight profile.

This type of display offers numerous advantages over a conventional strip chart. It provides immediate, at a glance, awareness of load levels relative to limits. If the lead structures engineer sees something of interest or concern, he can alert or query another engineer whose strip chart contains additional information for that surface. It also accommodates interdependent limits such as those represented by the clipped corners of the wing envelopes. In this area, the bending allowable is dependent on the current torsion value, and the converse is also true. With the strength envelope displayed, it is immediately evident whether a surface will be bending or torsion critical. Of more subtle, but equal, value is the ability to gain insight into certain loading characteristics. For example, in the lower half of Fig. 11(a), the asymmetric effects on the wing bending-torsion interactions are contrasted to the symmetric windup turn portion represented by the heavier area. Figure 11(b) shows data from an abrupt pullup that reached 6.2 g and 18° angle of attack. The nonlinear wing torsions associated with the aft center of pressure movement are evident as the buffet boundary and separated flow are encountered. Figure 11(c) illustrates the ability to compress a large amount of data from an extended period into one record, in this case, from 10 min of fairly aggressive air-to-air maneuvering. Other display possibilities are limited only by the real-time software program. For instance, comprehensive checking of all loads relative to limits could be displayed as color-coded bar segments for each component, or selected critical loads could be displayed as a function of load factor.

To summarize our experience with real-time monitoring and displays, a few comments are appropriate. Considering the number of potentially critical parameters for the X-29A aircraft, the display capacity was marginal but adequate and appropriate for the five engineers available for real-time monitoring. Numerous modifications and updates were required as different parameters became more-or-less critical during different test phases. While advanced graphic displays with cross-plotting capability can be extremely useful, they probably cannot totally replace conventional time histories for parameters such as high frequency buffet loads. Advanced computational and display capability is also no substitute for an experienced flight test team. Productivity and safety is enhanced by knowing what parameters will be critical for any given maneuver. This requires a proper blend of preflight and postflight analysis coupled with optimized displays.

Postflight Data Processing

Even with the great advances in real-time display capability, postflight data processing was required to extrapolate load levels to the next expansion point. Postflight data was processed on the Dryden mainframe computer and was generally available the next day after a flight. Basic data products included all load and basic aircraft parameters plotted as a function of time and/or load factor (typically 80 param-

6

eters for each maneuver). A useful and essential feature was the ability to overplot multiple maneuvers with or without predictions for comparison.

Maneuver Database Management

Because of the sheer volume of maneuvers, a relational database management system was implemented on a desktop computer. After each flight day, records were entered which contained information such as flight and card number, flight conditions, maneuver type, FCS mode, start and end times, maximum load factor, and angle of attack. The database could then be queried to provide sorting of data based on any combination of conditions. For example, the user could ask for all windup turns at Mach 0.6 that exceeded 10° angle of attack between flights 187 and 242. The X-29A structures database eventually totaled 3,086 "maneuvers," so the value of this type of database management system is apparent.

Load Prediction Capability

The ability to generate predictions for comparison to the flight-measured loads was an integral part of the flight test approach. This onsite capability was useful during the original envelope expansion and paid particular dividends when it came time to evaluate the planned FCS modifications. The prediction methodology was adopted and expanded from the methodology used by the contractor during the original external loads analysis from which the critical design conditions were generated. The methodology, as implemented at the NASA Dryden flight test site, is illustrated in Fig. 12. The foundation for the methodology is based on the availability of a database consisting of flexible unit loads that correspond to the flight load measurement stations. Similar to total aircraft stability and control derivatives, these unit loads describe the shear, bending moment, and torsion at each station due to each applicable effect, such as loading due to a unit change in angle of attack, flaperon position, canard position, rate damping terms, accelerations, and other effects.

The aerodynamic terms were developed from analytical models, corrected with rigid wind-tunnel data, and then flexibilized with the structural model. A complete set of derivatives was generated from the static aeroelastic analysis for each selected Mach number and altitude combination. Unit loads were available for the four wing stations, canard root, and vertical tail root stations. Unit loads were not available for the flaperon, strake flap, fuselage, discrete strain locations, or link loads. The original unit loads were based on early wind-tunnel data prior to the definitive NASA Ames Research Center wind-tunnel tests conducted in 1982. Because the unit loads were independent of angle of attack, predictions are not valid above moderate angles of attack, but the critical design conditions generally occur at high dynamic pressures where the trim variables are modest in value. Several updates to the unit loads were made as the flight test program progressed. These modifications and additions will be discussed in the results section.

By summing the individual terms for each station, load time histories are directly computed from trim and kinematic variables representing a discrete maneuver. As the prediction capability evolved, four options were available for generating the trim and kinematic variables as identified in Fig. 12. In the preflight mode, a trimmer program (option 1) could provide predicted trims for quasi-steady type maneuvers. The pilot-in-loop mission simulator (option 2) was the primary source for preflight analysis because of its ability to generate predicted kinematics for abrupt, asymmetric, or other untrimmed dynamic maneuvers. The kinematics were captured on a disk and transferred to the mainframe computer for later processing. Once a maneuver has actually been flown, the flight-measured kinematics (option 3) can be used for postflight analysis. This option provides valuable insight into the load prediction process because any difference between predicted and measured load should be caused by errors in the unit loads alone. Load predictions based on predicted kinematics are subject to errors in both the unit loads and kinematics, and it would be difficult to sort out the reasons for discrepancies without first evaluating the unit loads themselves.

Option 4 was added after a substantial flight database was available and proved especially useful for evaluating the new control laws. In this option, flight-measured stick positions are used to drive a batch simulation program to generate predicted kinematics. This process bypasses the need to use the manned simulation, which was in heavy demand for preflight pilot training, control law development work, and software verification and validation testing. A distinct advantage realized was that the predicted and flight-measured kinematics were based on a common set of control inputs, making the comparison of aircraft response more direct. To evaluate the new control laws, the same stick position time histories were input to different versions of the batch simulation. From these different simulation runs, overlays of the kinematics and computed loads could be compared for original control law predictions, revised control law predictions, and flight.

Preflight use of the prediction capability was extensive and included ACC and MCC windup turns, effects of maneuver rate and FCS downmodes, the extended maneuvers block of abrupt and asymmetric maneuvers, effects of the modified ACC schedules, and effects of the increased agility control laws. Of particular note are the MCC maneuvers and the evaluation of modified control laws, because these items were not included in the original design loads analysis. These preflight analysis tasks were performed by the onsite flight test team because of cost constraints and the fact that the original engineering design team was no longer intact because of the one–off nature of the program. The onsite prediction capability added measurably to the productivity of the flight program. A prime example was the modified ACC schedules, where preflight analysis provided the confidence to fly initial maneuvers to the 5.5-g level with followup maneuvers expanding back up to the 6.4-g limit. Similar gains were realized while reclearing the increased

7

agility control laws. While not a trivial task, an onsite prediction capability (through the use of existing simulator resources), can pay numerous dividends in flight productivity and interpreting flight test results. It is also the most viable way to keep up with an active and changing flight test program.

Key Results

General Loading Trends for the Wing

Typical wing loading trends with load factor are shown in Fig. 13 which compares measured data with the flight operating limits (FOLs) and two sets of predictions. One prediction is based on flight-measured kinematics and the other is based on simulator-predicted kinematics. The data are for the root wing station (WS) 31 from an ACC windup turn performed at Mach 0.9 and 10,000-ft altitude. These conditions were chosen because the transonic, high dynamic pressure region generated most of the wing critical design conditions and thus represents a more severe test of the prediction methodology. The flight-measured data are fairly linear with load factor and compare favorably with the 6.4-g FOLs, with the shear more critical than bending or torsion. At lower dynamic pressure conditions some of the loads (particularly torsion) could be very nonlinear because of flow separation at the higher angles of attack and because of ACC schedules that are not linear with angle of attack. The results shown in this figure are representative of the other wing stations. For this type of maneuver the root loads were generally more critical than those for the outer wing stations.

Predictions based on the flight-measured kinematics are somewhat nonconservative, showing lower slopes than the flight data and various errors at the 1-g level. While the overall correlation is considered reasonably good, these discrepancies indicate that modest errors exist in one or more of the unit load terms. Based on flight-derived parameter identification work (Ref. 13) and the static wing divergence analysis (Ref. 17), it is believed that both the angle of attack and flaperon unit load terms were underpredicted. More detailed analysis of flight data is required to isolate and quantify these terms. Simulator-based load predictions are overly conservative with the bending and shear intercepting their respective FOL well before the 6.4-g limit load factor. The significant differences in the two load predictions are directly attributed to trim differences between flight and the simulator because both predictions use the same set of unit loads. Generally, there is better correlation between predicted and flight-measured wing loads for subsonic and supersonic flight conditions.

Figure 14 illustrates the wing bending load trend with altitude at Mach 0.9. Data for the root station are extracted from ACC windup turns for constant load factors. Overall correlation between measured and predicted load is quite good. Both sets of data show a generally increasing trend, going from high to low altitude (increasing dynamic pressure), but the marked rise in the 1-g load level below an altitude of 15,000 ft for the prediction is not evident in the flight data.

This discrepancy may be caused by errors in the predicted basic airload distribution. The load increment between 1 g and 6.4 g for the flight data appears to be growing faster with decreasing altitude than indicated by the predictions. This trend is attributed to larger than predicted aeroelastic effects on the additional airload distribution and it is consistent with the proof test results that showed a slightly more flexible wing than predicted. More detailed research analysis is required to fully understand and quantify the reasons for these differences. The discrepancy between the flight and predicted data at 6.4 g and 30,000-ft altitude is caused by the extreme angle of attack required to generate limit load factor at such a modest dynamic pressure. The prediction is not expected to be valid at this condition because the unit load terms are independent of angle of attack. A number of differences exist between the measured and predicted wing loads. However, the overall methodology is considered validated for the design of a forward-swept wing that is subject to complex aerodynamic loadings and substantial aeroelastic effects.

General Loading Trends for the Canard

While flight results for the wing were favorable, such was not the case for the canard. Figure 15 illustrates general loading trends with Mach number for a constant altitude of 10,000 ft. Data are extracted and extrapolated from ACC windup turns for constant load factors. Dashed lines indicate both original and upgraded FOLs. The original FOLs were based on 80 percent of proof test values. The proof test loading was selected to represent the most critical 8-g maneuver load expected in flight. The FOL increase was possible because the canard was a stiffness design (as opposed to a strength design) and had substantial strength over what was proof tested. After analyzing flight load and pressure data, and reassessing the fuselage carry-through support structure, the bending FOL was increased to 100 percent of proof test value and the torsion FOL was set at 80 percent of the single hydraulic system capability (121 percent of proof test value). The original FOLs should ideally have provided a capability for 6.4-g subsonic and 5.2-g supersonic. As is evident from the shaded regions, limit load factor maneuvers generate flight loads that exceed the original 80 percent of proof values over a fairly broad Mach range for both bending and torsion. The high positive torsions are especially pronounced between Mach 0.9 and Mach 1, where limit load factor maneuvers would exceed the current hydraulic system cutoff. Flight restrictions were thus imposed in this region. Without the FOL increase, flight restrictions would have been necessary over a much broader Mach number and altitude envelope. Canard shear loads were in better agreement with predictions and the FOL, which indicates a more outboard and much more forward center of pressure than expected for transonic conditions. At supersonic Mach numbers, the positive torsions subside as the center of pressure begins to move aft of the spindle.

The adverse canard torsion characteristics in the transonic region are further illustrated in Fig. 16 which shows tor-

sion data as a function of load factor for windup turns at Mach 0.95. For flight data at 10,000-ft altitude, the hydraulic system limit is reached at approximately the 4.5-g level, whereas the prediction based on the original unit loads would indicate that there was no problem to the 6.4-g limit load factor. The slope of the flight data is approximately twice that of the original prediction. The original unit loads were generated prior to the definitive wind-tunnel tests conducted in 1982 at NASA Ames. An examination of that data indicated that the force and moment characteristics (particularly torsion) were highly nonlinear for transonic and supersonic Mach numbers. Compared to this data, the original linearized unit loads were nonconservative in representing the forward center of pressure location and probably should not have been linearized. In an attempt to improve the prediction capability, the unit loads were replaced in the prediction program with the nonlinear force and moment data. The revised predictions show a large improvement in the slope with load factor but a significant 1-g trim error compared to both flight data and the original prediction. The reason for the large intercept error is not understood at this time, but it is believed to be associated with the basic airload distribution at 0° angle of attack. At higher altitudes, the canard torsions presented no problems as shown by the flight data at 20,000-ft altitude. The nonlinear variation of the data is because of the higher angle of attack required to pull load factor at lower dynamic pressures. The very modest airfoil camber of the canard, combined with a strong upwash flow field from the wing, produces large changes in the chordwise pressure distributions because of flow separation at relatively low aircraft angles of attack (approximately 6° at Mach 0.95).

The more outboard and much more forward than expected center of pressure characteristics in the transonic region are primarily attributed to the low-aspect-ratio (1.47) planform of the canard. At modest angles of attack, flight data at Mach 0.95 indicate a spanwise center of pressure location approximately 50 percent of the exposed span. In addition, the chordwise center of pressure location is approximately 15 percent of the reference chord, which is not typical of more conventional higher aspect ratio surfaces. These characteristics appear similar to those documented in Ref. 19 for the YF-12A ventral fin which has an aspect ratio of 0.92. The adverse torsion characteristics of the canard also required a reassessment of the potential divergence tendencies, even though the predicted boundary was well outside of the flight envelope. A closed-form solution updated with "worst case" flight loads indicated that the canard divergence speed may be substantially less than originally estimated, but still outside the flight envelope. A cautious expansion at the lower altitudes eventually cleared the airplane to supersonic speeds.

Canard torsions (equivalent to hinge moments) were also of concern for supersonic, high dynamic pressure flight conditions, but for other reasons than discussed previously. Figure 17 shows the canard actuator load (proportional to the hinge moment) for 1-g trim trended with Mach number for altitudes from 40,000 to 10,000 ft. As the center of pressure moves aft of the spindle, a substantial portion of the negative hydraulic system FOL is required for the 1-g trim load. Extrapolated data for Mach 1.4 and 20,000-ft altitude indicate that the single hydraulic system capability would be exceeded during a 5-g pullup. This flight condition is within the structural design envelope which indicates that the chordwise center of pressure could be much more aft than expected at supersonic Mach numbers. The hydraulic system FOL is, in essence, limiting the maximum velocity permissible in a dive with pullup recovery.

An additional canard load characteristic that was not anticipated was the extreme sensitivity to sideslip for transonic and low supersonic Mach numbers at high dynamic pressures. Canard torsions were particularly sensitive, as shown in Fig. 18. The data are from full-pedal sideslip maneuvers performed across the Mach number range at an altitude of 20,000 ft. At Mach 1.1, the load increments from 1-g trim are large relative to the FOL for very modest angles of sideslip. This sensitivity is attributed to the shock cone angles relative to the leading-edge sweep which determines the extent of subsonic versus supersonic flow near the leading edge. An examination of the Ames wind-tunnel data substantiated this effect, and also indicated that the sideslip sensitivity would diminish around Mach 1.4 or at lower Mach numbers if the surface was sufficiently loaded due to angle of attack. Both of these effects were confirmed in flight. At high dynamic pressure conditions, small residual sideslip during nominal 1-g trim or at elevated load factors could cause noticeable differences between left- and right-canard hinge moments. For canard load predictions, the original matrix of unit loads did not contain terms due to sideslip, but were added to the prediction program based on flight-derived data.

The overall design methodology for the canard is judged as somewhat lacking, not because of its basic approach, but because of its attention to details. A less-than-comprehensive wind-tunnel database, available during the initial external loads analysis, also contributed to the deficiencies. Because of the significant asymmetric sideslip effects and 1-g trim loads that are large compared to the increment to pull load factor, one could question the validity of expecting 80 percent of design limit load factor to be achievable with FOLs based on 80 percent of the structural design limits. This question could be asked anytime a load is not linear with load factor, does not intercept zero load at zero load factor, or is sensitive to asymmetric effects which are not load-factor related. A number of additional examples which invite this question are shown in the following sections. A production airplane should not have this potential problem, because both FOLs and limit load factor would be based on 100 percent of design values.

General Loading Trends for the Wing Flaperon

Typical loading trends for the flaperon are shown in Fig. 19. Outboard flap actuator load is plotted as a function of load factor for two different maneuvers: a subsonic

9

symmetric windup turn and a transonic full-stick roll reversal initiated during a 5-g turn. Data from the subsonic windup turn is adversely nonlinear, primarily because of the heavy ACC control surface scheduling at Mach 0.6. While the load has approached the FOL at the 6-g level, the flap was near saturation (full-down position), and any additional increase in load factor would be expected to generate very little load increase. Data from the transonic maneuver show lower load levels for the symmetric windup turn portion because of the more moderate ACC schedules appropriate for this flight condition. The large asymmetric load increment caused by roll input is followed by a substantial aircraft unload prior to establishing the 5-g turn in the opposite direction. The aircraft unload is not caused by the pilot's inputs. The maneuver technique is to apply full lateral stick while maintaining constant longitudinal stick position, abruptly checking the roll when an equal and opposite bank angle is achieved. The unload is characteristic of the control laws which attempt to perform a roll about the aircraft velocity vector.

No predictions for the flaperon loads are shown because unit loads were not available in the original database supplied to the flight test team. To upgrade the prediction capability, unit loads derived from both the MCC and ACC flight data were added to the prediction routines. In general, the outboard flaperon loads appeared to be more critical for symmetric windup turn loadings, with the inboard flaperon loads more critical for asymmetric loadings caused by roll inputs. This characteristic may be caused by aeroelastic effects, as symmetric windup turn loadings tend to wash-in the outboard wing, placing it at a higher local angle of attack than the inboard wing. Asymmetric loadings caused by roll inputs would be expected to washout the outer wing, thereby relieving the flap loads relative to the inner wing (the classic aileron reversal tendencies of a trailing-edge device). During elevated g roll maneuvers, the combined wash-in and washout aeroelastic effects may be unique to a forward-swept-wing planform as used in the X-29A design. While some of the wing load characteristics tend to substantiate this premise, detailed analysis has not been completed, so this subject will not be addressed further. Some additional loading effects for the wing flaperons will be addressed in later sections of this paper.

Fixed Wing Flap Maneuvers

For various research purposes, MCC mode fixed-flap windup turns were flown over a broad envelope to help isolate the effects due to changing wing camber from those due to angle of attack variations. The normal ACC schedules lower the wing flap as angle of attack is increased, thus maintaining more balanced chordwise loadings which lead to lower wing torsions for a given load factor. As a result, the critical design load distributions are dependent on maintaining this expected balance. Preflight analysis of the MCC mode indicated that substantial increases in wing torsion could be anticipated for certain combinations of flap setting and flight condition. These penalties were confirmed

in flight as illustrated in Fig. 20, which shows wing torsions measured at the inboard swept station (WS 80) during windup turns flown at Mach 0.8 and 5,000-ft altitude. Data for the ACC mode is compared to the $-5°$ and $0°$ fixed-flap settings. The scheduled flap maneuver generates bending-critical load distributions, so the lower limit line applies, but it would not be reached before the 6.4-g load factor limit. As would be expected, the two fixed-flap maneuvers generate torsions with equal slopes with load factor but the data show a sizable offset. The fixed-flap slopes are climbing approximately twice as fast as the scheduled flap slope. Both fixed-flap maneuvers are torsion critical, so the upper limit line applies. While it would appear that additional load factor expansion would be possible for the $-5°$ fixed-flap maneuver, a flap-to-inner-wing link load, which was sensitive to both torsion and flap load, had reached its FOL, precluding any further expansion at this flight condition. In fact, the Mach 0.8 region at high dynamic pressures generated the most critical load penalties for the MCC mode. At lower dynamic pressures, the wing torsions would break nonlinearly prior to reaching the FOL, because of the higher angle of attack required to generate load factor. The MCC mode wing torsions also were not a problem at higher Mach numbers because of the naturally aft center of pressure movement.

An interesting side effect of the MCC mode was that, depending on flap setting, the canard could remain unloaded compared to the ACC mode which is designed to make the canard a major lift-sharing surface with the wing. In fact, for the $-5°$ fixed-flap maneuver shown in Fig. 20, both the canard and wing flap carried small down loads that remained virtually unchanged throughout the maneuver. This lack of load sharing also resulted in higher wing shear and bending loads for the same load factor compared to the ACC mode. The load and trim characteristics of the ACC mode are strongly driven by the highly integrated nature of the three-pitch-surface FCS-scheduled configuration, combined with the unstable airframe.

Abrupt Pitch Maneuvers

Preflight analysis indicated that maneuver onset rate would have a direct influence on the overall load distributions. Compared to slow windup turns, abrupt pullups to the same load factor were expected to generate higher wing loads but lower canard and flap loads. This influence was confirmed in flight. Figure 21 contrasts the differences in the kinematic "trim" state between the two types of maneuvers and the resulting wing loads as measured in flight at Mach 0.9 and 15,000-ft altitude. Limit load factor could be reached in under 1 sec for the abrupt pullup, compared to a nominal 20-sec onset specified for the windup turn. The different trim states (Fig. 21(a)) are attributed to the unstable airplane and the slow command rate of the ACC schedules. The abrupt pullup happens so fast that the FCS cannot follow the nominal ACC schedules, which results in less flap deflection and thus more angle of attack for a given load factor. The strength envelope for the wing (Fig. 21(b)) shows higher bending and torsion loads for the abrupt maneuver,

which is caused, in part, by the load sharing differences between the wing and canard for the two maneuvers. The trim state for the abrupt pullup also tends to increase the aeroelastic effects on the forward-swept wing, which leads to amplification of the wing loads, particularly for the outboard stations. In essence, the abrupt pullup maneuver tends to produce overall load distributions that are somewhat analogous to those for the MCC fixed-flap mode previously discussed.

The effect of maneuver onset rate on the canard loads is shown, for a different flight condition, in Fig. 22. For the slow windup turn, the ACC schedules generate a steady but somewhat nonlinear increase in canard load. The abrupt pullup results in a very nonlinear trend with load factor. After a modest up load to initiate the pitchup, the load reverses because of the unstable airframe. At peak load factor, a small down load is sufficient to arrest the pitch rate. Depending on flight condition, the initiation load at 1 g could be greater than the load at peak load factor. For this flight condition, the net result is maximum load levels which are approximately half of that for the slow windup turn.

The relatively slow-acting ACC schedules are probably undesirable from both performance and load viewpoints. The different trim states were particularly noticeable at low dynamic pressure conditions where the aircraft becomes angle-of-attack limited much more quickly because of the lagging flap deflection in an abrupt pullup. The clearance process is complicated by the need to deal with, in essence, two different aircraft. As mentioned earlier, the ACC schedule rate was intentionally kept slow to prevent interference with the pitch stabilization task. Simulator studies that were conducted indicated that some increase in the ACC rate would be possible, but this software update was not flight tested because of cost and time constraints.

Gross Weight and Center of Gravity Effects

Nominal mission profiles dictated that in-flight maneuver gross weights would range between 17,700 to 14,800 lb with a maximum center of gravity ($c.g.$) variation from -17 percent to -10 percent MAC. While these variations may seem modest, the heavy gross weight of 17,700 lb represents an 18-percent increase over the maneuver design gross weight. Thus, all maneuvers were flown to an equivalent load factor referenced to the 15,000-lb design weight. Beyond this first-order correction, it was originally thought that gross weight and $c.g.$ variations would have a small influence on the load distributions for the same equivalent load factor. However, as the military utility clearance got underway, it was deemed necessary to determine if certain gross weight and $c.g.$ combinations generated more critical load levels. An evaluation was conducted at several flight conditions for heavyweight/forward $c.g.$, midweight/aft $c.g.$, and lightweight/mid $c.g.$ configurations. These combinations bracketed the normal fuel burn sequence. Maneuvers repeated for each combination included slow windup turns, abrupt pullups, 360° rolls initiated at 1 g, and elevated g roll reversals.

Aft $c.g.$ maneuvers generated significantly higher wing flaperon loads as illustrated in Fig. 23, which compares the inboard flaperon pushrod load variation during two slow windup turns. The negative load axis indicates that the pushrod is in compression for an uploaded flaperon. It should be noted that the increase in load level of approximately 15 percent at limit load factor resulted from a modest 6 percent-more-aft $c.g.$ position. For this flight condition, the more critical aft $c.g.$ load levels could be accommodated for symmetric windup turns to the limit load factor. But the additional asymmetric load increments caused by roll reversals produced a total load that reached the FOL for reversals initiated at the 4-g level. Roll reversals at the 5-g level could be cleared for a forward $c.g.$ but not for an aft $c.g.$ within the existing FOL. The inboard flaperon pushrod load was the most critical parameter for elevated g roll reversals. It was naturally desirable to have a maneuver envelope clearance that was not dependent on fuel state, which would require that all additional roll reversal clearance be conducted at the critical aft $c.g.$ Fortunately, in the middle of the military utility clearance activity, the revised ACC schedules were implemented and a somewhat unplanned byproduct of the ACC schedule change was a reduction in the flaperon trim loads for a slow windup turn. This reduction offset the $c.g.$ effect and allowed 5-g reversal clearance to be completed for the critical aft $c.g.$ condition. The revised ACC schedules will be discussed in more detail later.

For windup turn and abrupt pullup maneuvers, the heavyweight/forward $c.g.$ configuration generated slightly higher wing loads overall (approximately 3 percent). This percentage is consistent with that expected from inertia relief effects for a configuration without a wet wing such as the X-29A aircraft. Not anticipated was a large increase in canard loads, up to 20 percent for the heavyweight/forward $c.g.$ compared to the midweight/aft $c.g.$ configuration. Thus, all additional windup turn and abrupt pullup clearance was performed at a heavyweight/forward $c.g.$ position. Characteristics during 360° rolls did not appear to be sensitive to weight and $c.g.$ variations. The lightweight/mid $c.g.$ configuration was not critical for any maneuver type.

The wing flaperon and canard trim loads sensitivity to small $c.g.$ changes was not anticipated prior to flight test and is attributed to the ACC schedule implementation, combined with the relatively small moment arms between the $c.g.$ and these primary trimming surfaces. (The estimated arms are 0.5 MAC for the wing flaperon and 0.9 MAC for the canard.) The load sensitivities to gross weight and $c.g.$ variations put constraints upon, and greatly complicated, the flight-planning process.

Flight Control System Backup Mode

As mentioned in the aircraft description section, the analog reversion (AR) backup mode was not designed for large amplitude aggressive maneuvering about any axis. Even so, the AR mode had to be cleared for FCS stability and aeroservoelasticity in case of an inadvertent downmode from the

normal digital (ND) mode. Clearance was obtained over the full envelope through the 1-g ITB-1 described earlier. In the ND mode, canard and strake flap positions are nominally set at modest negative angles at 1-g trim. For simplification in the AR mode, the canard and strake flap reference positions are set to 0°, independent of angle of attack and flight condition. The net result is that for 1-g trim, the AR mode commands increased control surface incidence compared to the ND mode. The wing flaperons also move more trailing edge down to force the canard to the nominal 0° position. While of no consequence at low dynamic pressures, the transonic expansion at lower altitudes began to reveal significant 1-g trim load penalties for the canard and flaperon because of the "overcambered" surface positions at high dynamic pressures.

Figure 24 shows typical time histories for the canard actuator load, contrasting the difference in the two modes. The time histories were taken from the longitudinal stick frequency sweeps that are performed for the real-time FCS phase and gain determination. The stick inputs consist of small amplitude oscillations of increasing frequency until the pilot's arm is rate limited. Note that the mean trim load has increased by a factor of approximately 2.5 for the AR mode. Both time histories represent load factor excursions from approximately 0 to 2 g. For the AR mode, the resulting peak canard actuator load reached two-thirds of the hydraulic system FOL, which is significant for a 2-g maneuver. For the canard actuator load, the differences between the two modes were most evident in the critical Mach 0.95 region where the AR mode added to the problems discussed previously. At this flight condition, the AR mode had a 3-g load factor restriction.

In Fig. 24 it is also interesting to note the difference between the modes in the higher frequency content superimposed on the lower frequency oscillations. This content represents the dynamic activity of the actuator required to stabilize the highly unstable airframe, and is particularly evident for the ND mode in the last 8 sec where the pilot had completed the stick frequency sweep. The AR mode displays a lower overall frequency content but slightly higher amplitudes. In either mode, the canard is never allowed to stop moving. The high dynamic activity of the canard actuator load raised some concerns relative to free play and fatigue life of the actuator rod end. In fact, to minimize wear, it became standard practice to select the lowest gain AR mode during aircraft taxi because of sensor feedback.

As noted earlier, the AR mode also commands more trailing-edge-down wing flaperon deflection for 1-g trim. Inboard flaperon trim load penalties were especially severe for low-altitude supersonic conditions where the flaperon has to work much harder to generate nosedown pitching moments. For 1-g trim in the AR mode, inboard flaperon pushrod load levels were projected to reach the FOL for low supersonic Mach numbers at 5,000-ft altitude. Prior to flight testing, the significance of the AR mode trim differences was not fully appreciated. The structural design analysis

did not address the AR mode. It would seem desirable, in principle, to have a backup FCS mode that trims the aircraft similar to the primary mode. Thus, a better choice for the canard reference position in the AR mode would have been something more negative that approximated the ND mode.

Buffet-Induced Loads

The flight envelope where buffet-induced loads were a consideration included airspeeds up to 350 KEAS for subsonic and transonic Mach numbers. Data up to the 20° angle-of-attack limit were generally obtained between airspeeds of 200 to 300 KEAS. The primary test matrix for buffet research consisted of slow onset windup turns in both the ACC mode and the MCC fixed-flaperon mode covering the Mach 0.6 to 0.95 range at a reference dynamic pressure of 275 lb/ft². The most significant buffet loads were measured on the wing flaperon surfaces during the ACC maneuvers. Time histories from the maneuver that generated the highest peak dynamic loads on the outboard and inboard flaperon are shown in Fig. 25. Target conditions for this maneuver were Mach 0.7, 275 lb/ft² dynamic pressure, and 15° angle of attack. Both flaperons reached full down saturation around 10° angle of attack and remained in this position through peak angle of attack. Note also that the dynamic pressure was increasing during the maneuver. The inboard flaperon shows a very sharp rise in intensity, with a considerable overshoot of the FOL at 16° angle of attack. This data was processed at 400 samples/sec and though not evident from the compressed time scale, the inboard flaperon was responding at its primary structural frequency of 28 Hz. Note that the mean load is not excessive (64 percent of the FOL) but the peak dynamic load cycles from almost 0 to 120 percent of the FOL. By contrast, the outboard flaperon shows a much higher mean load (86 percent of the FOL) but considerably lower dynamic activity (peak-to-peak load is 46 percent of the FOL), which is still significant.

The lower buffet intensity for the outboard flaperon is attributed to the relatively cleaner flow expected in the tip region for a forward-swept wing. Accelerometer data has shown that the canard encounters buffet onset before the wing, and it is surmised that the inboard flaperon buffet intensity is sensitive to the level of flow separation present on the canard, because of its close proximity to the wing-root region. Buffet-induced loads measured on the wing, canard, and vertical tail structures generated no concerns. To put the flaperon buffet loads in perspective, it should be pointed out that buffet load levels for the wing itself were considered typical of other aircraft — peak-to-peak dynamic bending loads in the 8 to 10 percent of FOL range. It has proven difficult to analyze and quantify the buffet intensity characteristics because of the many variables involved which include Mach number, dynamic pressure, angle of attack, flaperon position, and canard position. The ACC trim variables are sensitive, not only to flight condition, but also to maneuver onset rate and smoothness. Rapidly changing flight conditions, because of the thrust-deficient nature of the maneuvers, made for a difficult piloting task.

Buffet intensity characteristics of the flaperon were of concern, not only because of the high peak loads that were experienced, but also because of the potential impact to the airplane's fatigue life. The X-29A aircraft was designed for a service life of 3,000 hr·using accepted damage tolerance concepts, but the analysis did not specifically address buffet-induced loadings. As a research vehicle, the X-29A aircraft was only expected to accumulate several hundred hours of flight time. Nevertheless, after a sufficient buffet database had been established, a reanalysis of the fatigue damage rate was performed using the flight data. This analysis confirmed that the inboard flaperon was indeed the fatigue-critical component. Based on the maximum damage rate sustained at peak load levels at or near the FOL, the fatigue life of the inboard flaperon structure was estimated to be only 6 hr. Assuming the average buffet maneuver produced 15 sec of exposure at maximum buffet intensity, the 6 hr of fatigue life would equate to 1,440 heavy-buffet maneuvers. This number is more than adequate for the planned usage of a research vehicle such as the X-29A aircraft, but would probably be of concern for an operational fleet aircraft.

Revised Control Surface Schedules

The original ACC schedules were modified with three objectives in mind: (1) reduction of canard positive torsion loads in the transonic, high dynamic pressure region; (2) reduction of canard negative torsion loads in the supersonic, high dynamic pressure region; and (3) improvement in the aircraft buffet characteristics at high angles of attack in the subsonic and transonic, low dynamic pressure region. Improvement in overall aircraft aerodynamic performance was not an objective. To minimize the number of changes, only the tables of canard position as a function of angle of attack were modified at the Mach number and altitude breakpoints appropriate for each of the three objectives. Modifications were not allowed to the tables of strake flap position as a function of wing flaperon position.

It was realized that these simplifications would compromise the first objective because the revised schedules would result in an overall "decambering" of both the canard and wing flaperon surfaces. For a given load factor, the canard position would be more negative, the wing flaperon position less down, and thus a higher angle of attack would be required for the revised schedules. With the canard loads driven more by angle of attack than canard position, little, if any, canard load relief was expected for slow windup turns in the transonic region. Maneuvers flown with the modified ACC schedules showed no relief in the canard torsion load levels compared to the original ACC schedules, so data comparisons will not be shown. Some canard load relief probably could have been obtained by taking advantage of the flexibility offered by the three-surface pitch control. This approach would have required extensive changes to the strake flap tables to preclude the higher angles of attack resulting from the lower wing flaperon settings. Because the higher than expected canard loads dictated some

flight restrictions in the transonic, high dynamic pressure region, the more extensive changes to the ACC schedules would have been justified, but were precluded because of time constraints.

Existing flight and wind-tunnel data indicated that ACC schedule changes in the supersonic region (objective 2) probably would not provide much relief in the canard negative torsion load levels. At low supersonic Mach numbers around 1.2, changes in angle of attack or canard position had a small influence on the total canard torsion because the center of pressure for these loading effects is relatively close to the spindle. Thus, the load distribution is dominated by the basic loading at 0° angle of attack. The limited amount of supersonic flight data obtained with the revised schedules was insufficient to confirm the expected effects of the schedule changes. Alternatives to modify the supersonic characteristics would include changes to the canard planform or camber shape, or the addition of a scheduled flap to the canard itself.

Flight data from ACC windup turns indicated that the canard surface encountered buffet onset before the wing. By modifying the canard schedule with angle of attack, an improvement in the overall aircraft buffet characteristics possibly could be realized (objective 3). Canard buffet loads were not a concern from a structural viewpoint, however, a reduction in the level of canard flow separation might have a beneficial effect on the adverse buffet characteristics of the inboard wing flaperon described in the previous section. Figure 26 shows a comparison of the buffet response of the inboard flaperon recorded during two windup turns flown before and after the ACC schedule change. The dynamic load data were corrected to a common reference dynamic pressure of 275 lb/ft^2 and plotted as a function of angle of attack at 400 samples/sec. Thus at any given angle of attack beyond the flaperon saturation point, the only difference between the two maneuvers should be the canard position. In the 16° to 17° angle-of-attack range where the peak dynamic activity occurs, the canard position is 4° more negative for the modified schedule data. Within the limited evaluation possible with these two maneuvers, it appears that the modified ACC schedule generated approximately 5 percent higher mean flaperon loads, but with a substantial reduction in the dynamic load levels of about one-third. A reduction in the buffet response was also seen at subsonic Mach numbers where the revised ACC schedules allowed higher angles of attack to be achieved before reaching the FOL. The reduced level of dynamic activity would also directly result in lower fatigue damage rates.

Increased Roll Agility Control Laws

In the original control law implementation, roll rates and accelerations were intentionally kept conservative to minimize potential roll-pitch coupling tendencies during the initial envelope expansion phase. For the final military utility and agility testing, it was desirable to increase the roll performance to levels comparable to those of current fighter aircraft. Since the baseline control laws showed good roll

13

coordination, an FCS software update was flight tested that substantially improved the roll performance (both acceleration and maximum rate) in the heart of the military utility envelope. The effect of the increased roll agility control laws on the most critical structural load parameter is illustrated in Fig. 27. The inboard flaperon pushrod load generated by full stick roll reversals initiated at the 5-g level is shown for the Mach number range cleared at an altitude of 10,000 ft. It should be noted that the 5-g symmetric trim load is not affected by the control law change so only a single line is shown. Although the roll rate increase is substantial at Mach 0.6, the maneuver with revised gains did not produce an increase in the load increment due to roll for the down-moving flaperon, because the flaperon was already saturated full down for the maneuver with the original gains. All of the increased roll rate was generated by the up-moving flaperon which did not present a problem. Flaperon saturation could result from the combination of symmetric deflection caused by the ACC schedules and the additional asymmetric movement caused by roll inputs. At Mach 0.7 and 0.8, a load penalty for the revised gains is registered because the flaperon was not saturated for the maneuvers with original gains. Note that the load penalty resulting from the revised gains is slightly larger at Mach 0.8 compared to Mach 0.7 even though the roll rate increase is less. This characteristic is common to trailing-edge devices because the control surface has to work harder to generate a given roll rate as Mach number increases. At Mach 0.8, the revised gains produced an increase in the load increment due to roll of approximately 22 percent, which is greater than the percentage increase in roll rate.

With the peak reversal loads already at, or slightly over, the original FOL for the baseline control laws, it was necessary to upgrade the FOL prior to clearing the revised control laws. This FOL upgrade was also desired to accommodate the trim loads expected during additional supersonic, low-altitude expansion and the high buffet loads described earlier. The proof test on the flaperon represented load levels considerably lower than the original design values because of control law changes that occurred after the structural design was completed. However, the pushrod load was the only parameter for the inboard flaperon being measured in flight, and it was realized that other parts of the flaperon structure could possibly be more critical than the pushrod itself. Therefore, it was necessary to reinstall four additional strain gages located on the hinge fittings which duplicated measurements available during the proof test. With real-time monitoring of the additional four measurements, along with the pushrod load, it was justified to increase the FOL to 100 percent of the proof test value.

Increased Pitch Agility Control Laws

The pitch agility capabilities were intentionally constrained in the original control law implementation because of concern for the highly unstable airframe. With an extensive flight database from previous clearance efforts providing a foundation, it was concluded that substantial increases in the pitch agility characteristics could be safely accommodated from both a control system and structural loads viewpoint. Preflight analysis indicated that maneuver initiation loads would increase for the revised control law gains, but at limit load factor conditions, very little load penalty would be realized because the limit load factor remained unchanged.

As expected, the largest load penalties resulting from the increased pitch agility control laws were measured on the canard. A typical example is shown in Fig. 28 which shows the comparison of the bending moment from abrupt pullups performed before and after the control law revision. The maneuver initiation load is noticeably higher for the revised gains, but the peak levels remain low relative to the FOL for the same reasons discussed previously in the section dealing with abrupt pitch maneuvers. Wing loads did not show significant penalties at the higher load factors. The maneuver flown with the revised gains represents an increase in peak pitch acceleration of about 25 percent compared to that generated with the original gains. Pitch onset quantities cannot be stated in absolute terms because of data dissemination restrictions. It would appear, at least from a loads perspective, that additional pitch onset increases would be possible at this flight condition, as long as the FCS capabilities remain adequate for controlling the unstable airplane. In fact, at Mach 0.6 the pitch acceleration was increased by 58 percent over the original gains with load penalties no more significant than those shown for the Mach 0.8 condition. The pitch onset capability was one of the major benefits expected from the three-surface pitch control combined with the unstable airframe. In contrast to the roll agility improvement, the pitch onset characteristics were significantly improved, with the associated load penalties easily accommodated within the existing structural limits.

Concluding Remarks

To support the many research objectives of the X-29A project, structural loads clearance was a necessary activity throughout the flight test program. Symmetric load factor clearance was accomplished over a broad envelope in both the control surface scheduled mode and the fixed-flaperon mode. Abrupt and asymmetric maneuvers were cleared over a limited envelope in support of the military utility and agility testing. The size of this envelope had to be traded off against the desire to reclear the envelope with updated flight control laws. The bulk of the structural loads flight testing was designed to provide maneuver clearance, but by its very nature it has provided an extensive database for correlation and evaluation of the load prediction methodology. Development of a load prediction capability, interfaced with the simulator, was considered an important accomplishment that played a key role toward increasing flight test productivity and understanding some of the load characteristics. Fixed-flaperon testing, in particular, has generated data that may allow the discrete loadings due to angle of attack, flaperon position, and canard position to be isolated for comparison to the predicted unit load coefficients.

14

No significant problems were encountered with structural loads related to the forward-swept wing or the composite structure. This area received a great deal of attention in the analysis, design, and test phases. While the overall design methodology was considered validated, a number of structural load characteristics were not adequately predicted. The low-aspect-ratio canard experienced higher than expected loads, particularly hinge moments. Control surface trim load sensitivity to center of gravity position, effects of the backup flight control system mode, and the buffet intensity characteristics of the wing flaperon surfaces represent three areas where the structural load characteristics were not fully anticipated prior to flight test. Evaluation of the revised control surface schedules produced mixed results. Testing of the increased pitch agility control laws was accommodated with virtually no impact on the structural loads, but the increased roll agility control laws could not be accommodated within the original structural limits. Many of the load characteristics were dictated by the control laws, which emphasizes the need for high quality measurements of airdata, angle of attack, and control surface positions because these quantities are key inputs to the flight control system. Comprehensive measurement of all control surface loads is recommended for an advanced control configured vehicle such as the X-29A aircraft.

Conventional flight testing techniques, utilizing a conservative buildup approach, were adequate to insure flight safety. However, advanced analysis techniques, real-time displays, and an onsite load prediction capability were needed to keep pace with an active and changing flight test program. A simulator-based prediction capability, in particular, appears to be the most viable means of coping with a highly integrated design that has flight characteristics dominated by the programmable control laws. This trend in aircraft design seems to be accelerating, even for configurations that do not incorporate technologies as radical as those in the X-29A aircraft. Several examples were shown where an evolving control law design affected the critical design loads, the proof test, and ultimately the flight operating limits. In the case of the canard and flaperon structural limits, early control laws resulted in additional strength over what was proof tested. The reverse situation could be true in other cases, as illustrated by the increased roll agility control laws. A number of load characteristics not proportional to load factor were illustrated, which brings into question the validity of expecting 80 percent of design limit load factor to be achievable with structural limits based on 80 percent of design values. Prior to flight test, the primary structural concern was obviously the forward-swept wing, but perhaps more lessons were learned in other areas. As was true for the other technical disciplines, structural flight testing of the X-29A aircraft provided the opportunity and need to reevaluate our approach to testing a unique and unconventional aircraft.

References

1. Krone, N.J., Jr., "Forward Swept Wing Flight Demonstrator," AIAA-80-1882, Aug. 1980.

2. Spacht, G., "The Forward Swept Wing: a Unique Design Challenge," AIAA-80-1885, Aug. 1980.

3. Grumman Aerospace Corporation, "X-29A Aircraft," AFWAL-TR-85-3099, vol. 1-4, Bethpage, New York, March 1987.

4. Trippensee, Gary A., and David P. Lux, *X-29A Forward-Swept-Wing Flight Research Program Status*, NASA TM-100413, 1987.

5. Hicks, John W., James M. Cooper, Jr., and Walter J. Sefic, "Flight Test Techniques for the X-29A Aircraft," AIAA-87-0082, AIAA 25th Aerospace Sciences Meeting, Reno, Nevada, Jan. 12–15, 1987. Also published as NASA TM-88289, 1987.

6. Hicks, John W., and Kevin L. Petersen, "Real Time Flight Test Analysis Techniques for the X-29A Aircraft," AGARD FMP 73rd Flight Test Techniques Symposium, Edwards A.F.B., Oct. 1988.

7. Hicks, John W., and Neil W. Matheny, "Preliminary Flight Assessment of the X-29A Advanced Technology Demonstrator," AIAA-87-2949, AIAA/AHS/ASEE Aircraft Design, Systems and Operations Meeting, St. Louis, Missouri, Sept. 13–16, 1987. Also published as NASA TM-100407, 1987.

8. Ishmael, Stephen D., and Lt. Col. Ted Wierzbanowski, "X-29 Initial Flight Test Results," Society of Experimental Test Pilots 29th Symposium, Sept. 1985.

9. Smith, Rogers E., and Kurt C. Schroeder, "Flight Testing the X-29," Society of Experimental Test Pilots 30th Symposium, Sept. 1986.

10. Bosworth, John T., *Flight-Determined Longitudinal Stability Characteristics of the X-29A Airplane Using Frequency Response Techniques*, NASA TM-4122, 1989.

11. Gera, Joseph, and John T. Bosworth, "Dynamic Stability and Handling Qualities Tests on a Highly Augmented, Statically Unstable Airplane," AIAA-87-2258-CP, AIAA Guidance, Navigation and Control Conference, Monterey, California, Aug. 17–19, 1987. Also published as NASA TM-88297, 1987.

12. Butts, 1st Lt. Stuart L., and 1st Lt. David M. Rajczewski, *Flying Qualities Evaluation of the X-29A Research Aircraft*, AFFTC-TR-89-08, May 1989.

13. Budd, Gerald D., and Neil W. Matheny, *Preliminary Flight Derived Aerodynamic Characteristics of the X-29A Aircraft Using Parameter Identification Techniques*, NASA TM-100453, 1988.

14. Huckabone, Capt. Thomas C., and Todd H. Snyder, *Performance Evaluation of the X-29A Research Aircraft*, AFFTC-TR-87-51, March 1988.

15. Hicks, John W., Jan Kania, Robert Pearce, and Glen Mills, "Challenges in Modeling the X-29A Flight Test Performance," AIAA-87-0081, AIAA 25th Aerospace Sciences Meeting, Reno, Nevada, Jan. 12–15, 1987. Also published as NASA TM-88282, 1987.

16. Hicks, John W., and Bryan J. Moulton, "Effects of Maneuver Dynamics on Drag Polars of the X-29 Forward-Swept-Wing Aircraft With Automatic Wing Camber Control," AIAA-88-2144, Fourth Flight Test Conference, San Diego, California, May 18–20, 1988. Also published as NASA TM-100422, 1988.

17. Schuster, Lawrence S., and William A. Lokos, *Current Flight Test Experience Related to Structural Divergence of Forward-Swept Wings*, NASA TM-100445, 1988.

18. Skopinski, T.H., William S. Aiken, Jr., and Wilber B. Huston, *Calibration of Strain-Gage Installations in Aircraft Structures for the Measurement of Flight Loads*, NACA Rept. 1178, 1954.

19. Meyer, Robert R. and V. Michael DeAngelis, *Flight-Measured Aerodynamic Loads on a 0.92 Aspect Ratio Lifting Surface*, NASA CP-2054, vol. 1, 1978.

Fig. 1 X-29A airplane.

Wing flaperons
Canard
Nose strakes
Strake flap
48 ft 1 in.
F-5A nose section
Rudder
14 ft 9.5 in
Strake flap

Wing area = 185 ft^2
MAC = 86.6 in.
Aspect ratio = 4.0
Taper ratio = 0.4
Sweep angle (leading edge) = -29.3 deg
Gross weight (take off) = 17,800 lbs

27 ft 2.44 in.

6247
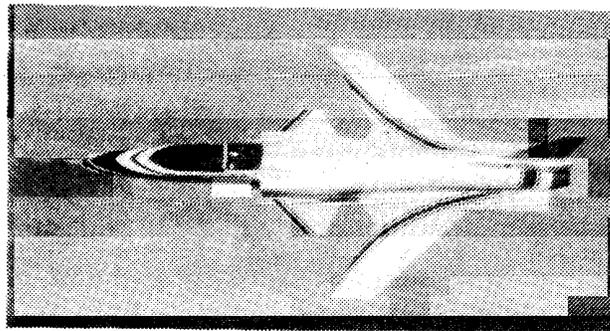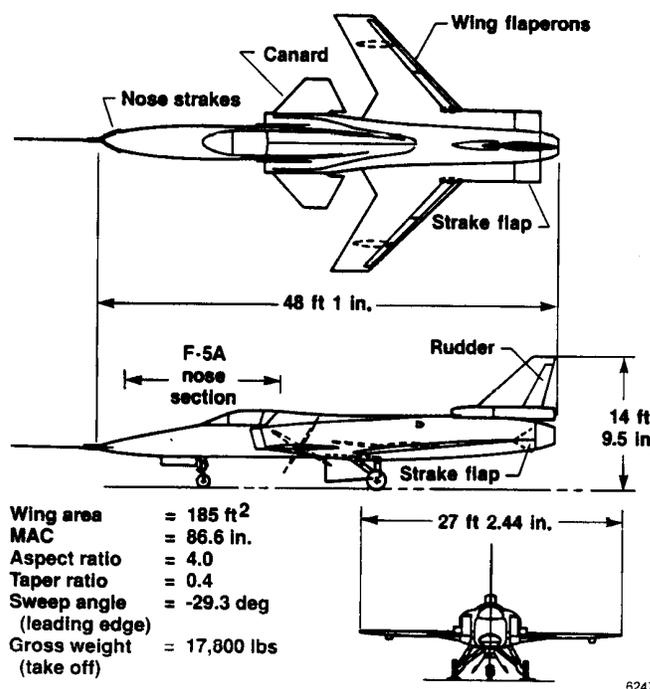
Fig. 2 X-29A airplane, three views.

16
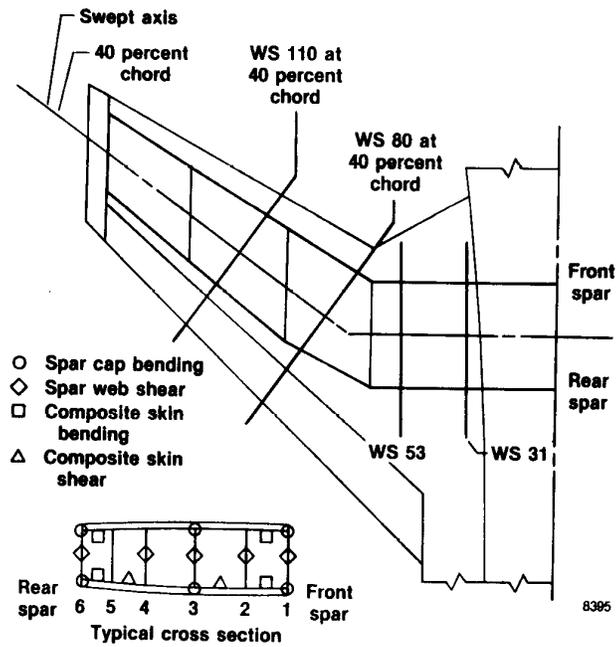
Fig. 3 X-29A wing load measurements.

Fig. 4 Canard load measurements.

17

	1985	1986	1987	1988
Limited envelope phase • ITB-1, ITB-2 – Minimum maneuvering Flight 1 △ • Symposium (14 Dec 84) • Aircraft layup for FCS update	▄▄▄▄ △ Flight 16 △ ▢			

Envelope expansion phase
• ITB-1, ITB-2, divergence clearance
  – Windup turns, sideslips, 1-g rolls   Flight 17 △
• Industry briefings
• Aircraft layup for instrumentation/calibrated
   engine installation
		▄▄▄▄▄▄▄	△ Flight 104
			▢
			▭	

Follow-on research phase
• Performance, buffet, pressure distributions,
   parameter identification, divergence research
  – Continued windup turn expansion
• Military utility agility evaluation
  – Abrupt pullups, roll reversals, rudder reversals
• Revised ACC schedules
  – Reassessments, continue loads clearance
• Increased pitch/roll agility
  – Reassessments, continue loads clearance
• Final flight of aircraft #1 program
			Flight 105 △
			Flight 140△
				▄▄▄▄▄▄▄
				
				Flight 187 △
				Flight 214△
				Flight 242
				(8 Dec 88) △

9881

Fig. 5 Flight test chronology.
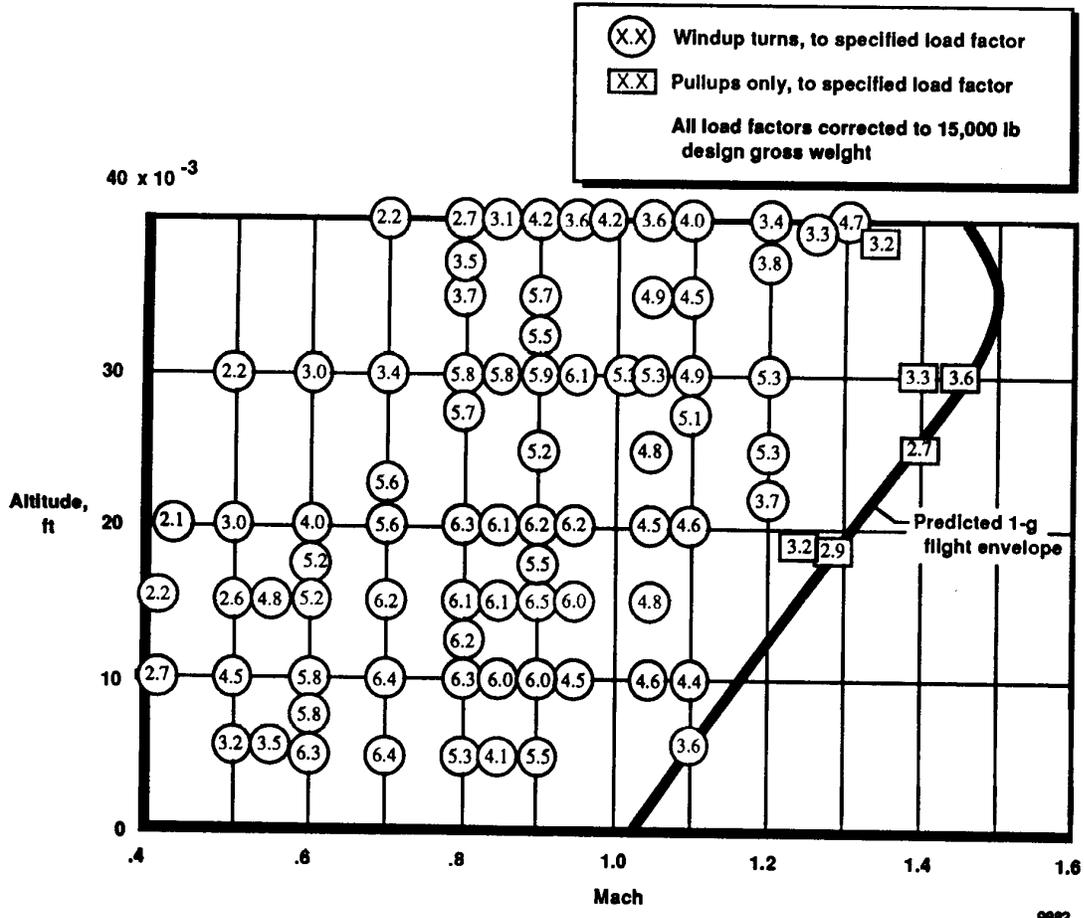
Fig. 6 Windup turn test matrix, ACC mode.
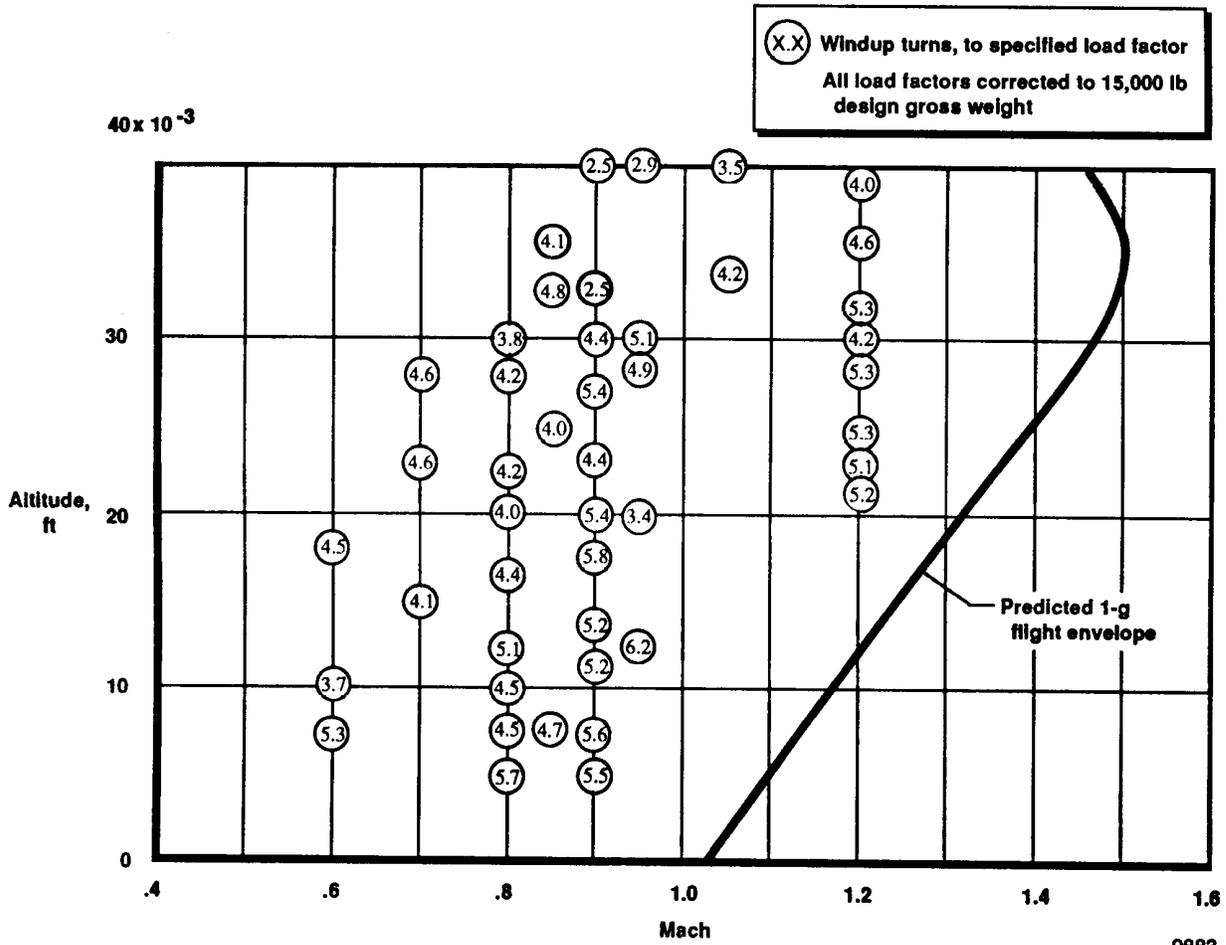
Fig. 7 Windup turn test matrix, MCC mode, 0° fixed wing flap.

9883
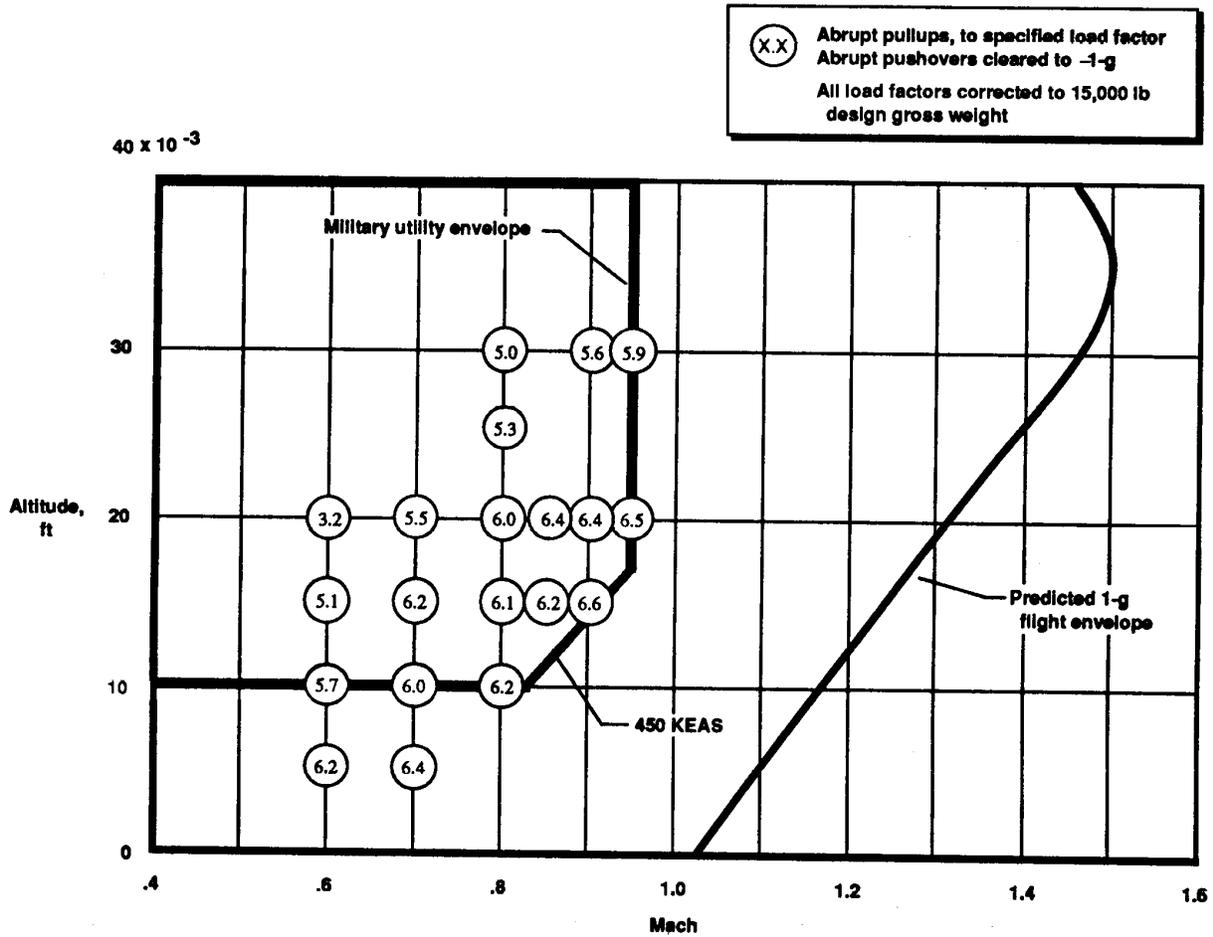
Fig. 8 Abrupt pullup–pushover test matrix, ACC mode.
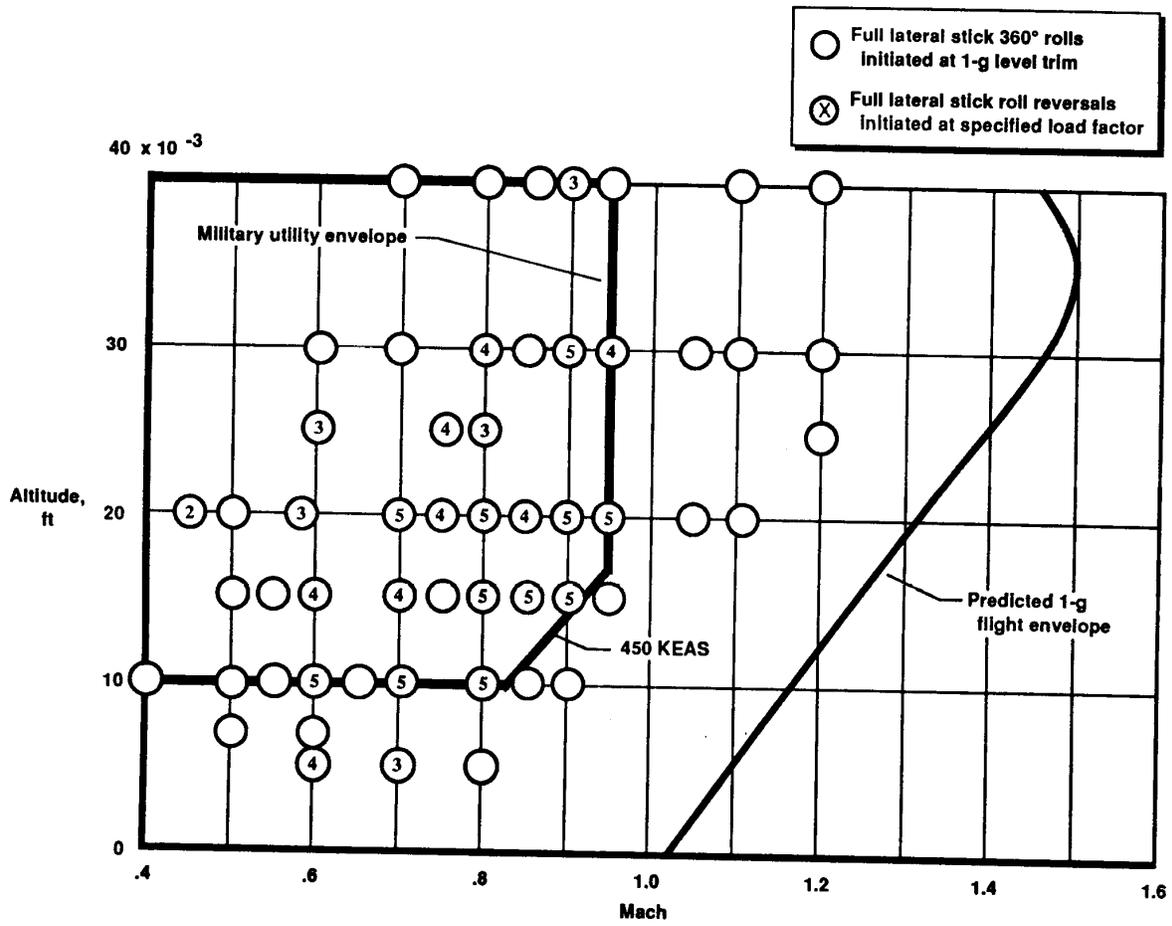
Fig. 9 Rolling maneuvers test matrix, ACC mode.
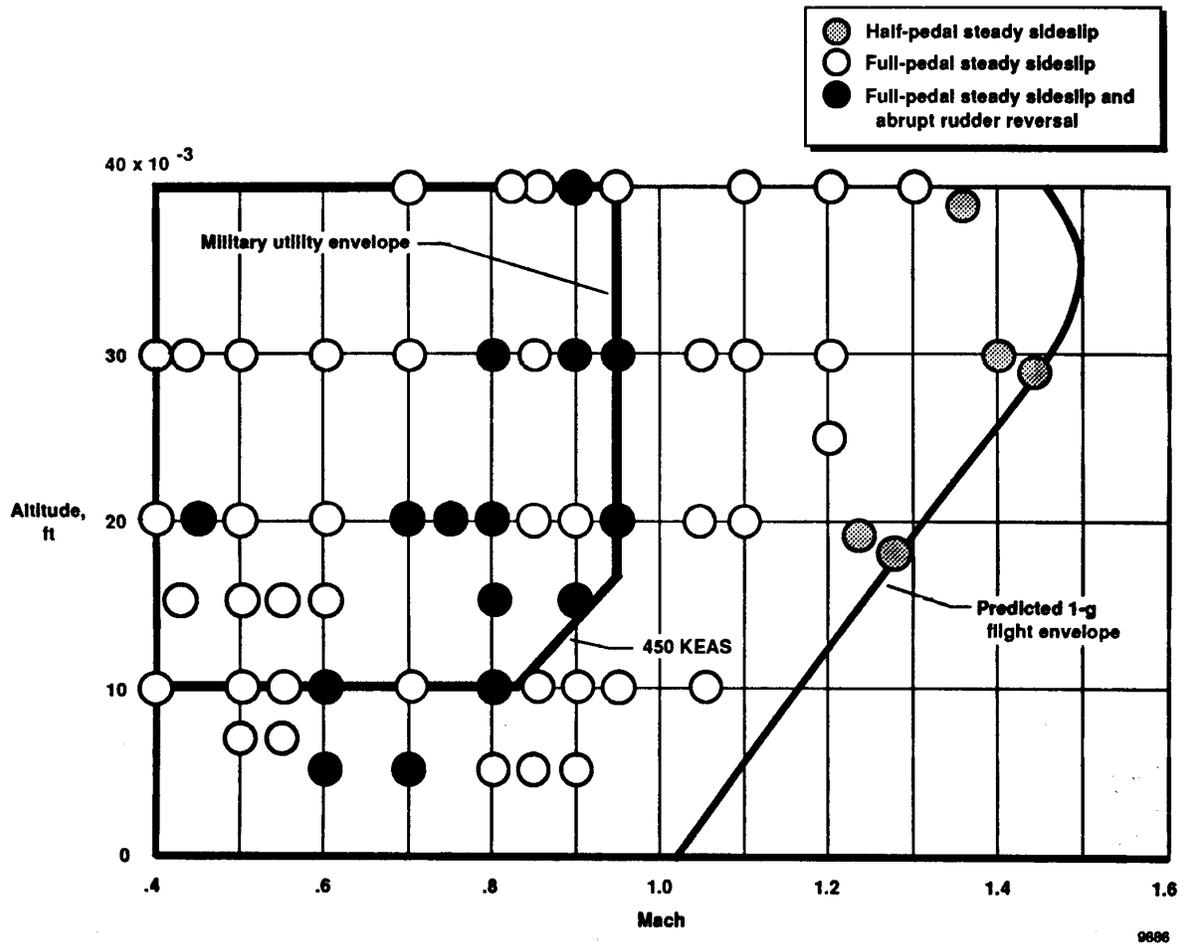
Fig. 10 Directional maneuvers test matrix, ACC mode.
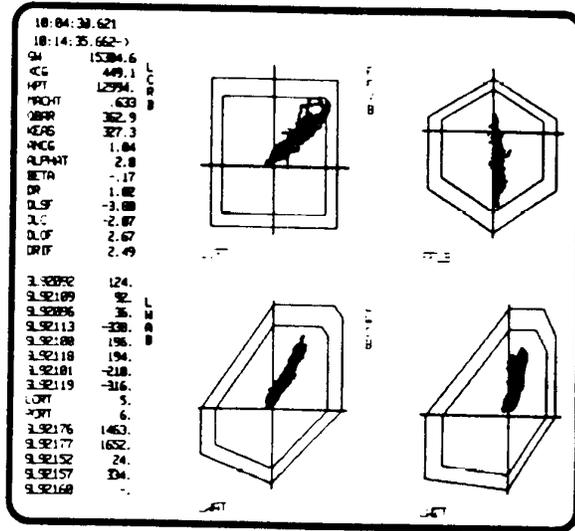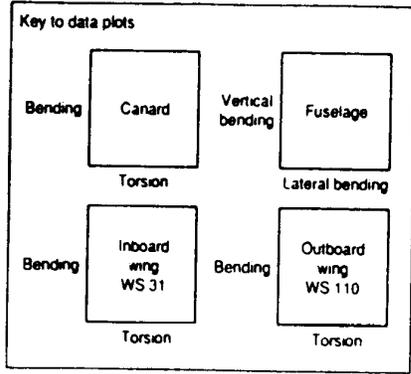
(c) Military utility air-to-air maneuvering.
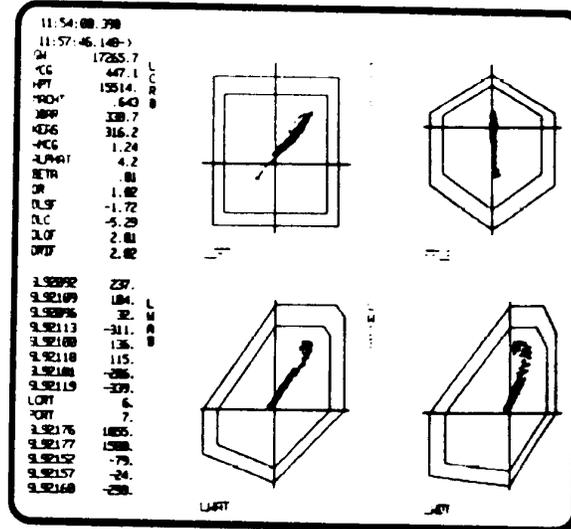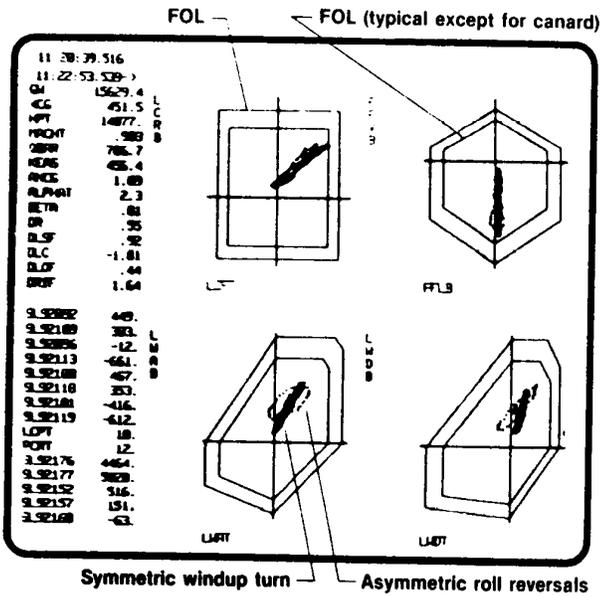
(a) Roll reversals; $M = 0.9$, $h = 15,000$ ft, $N_Z = 5.0$ g.

(b) Abrupt pullup; $M = 0.7$, $h = 15,000$ ft, $N_Z = 6.2$ g, $\alpha = 18°$.

Fig. 11 Real-time graphics display of strength envelopes.
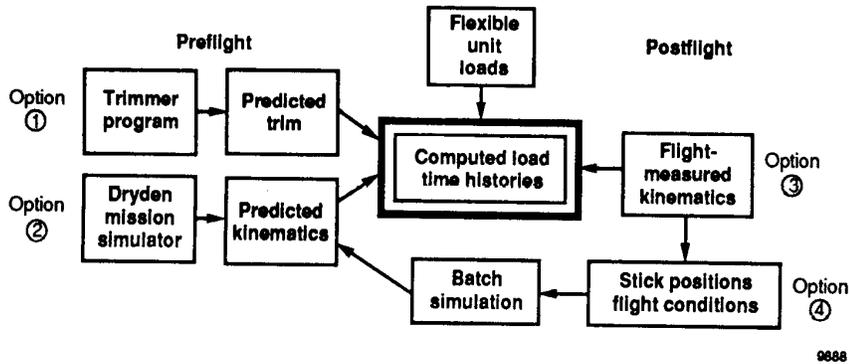
Fig. 12 Load prediction methodology.
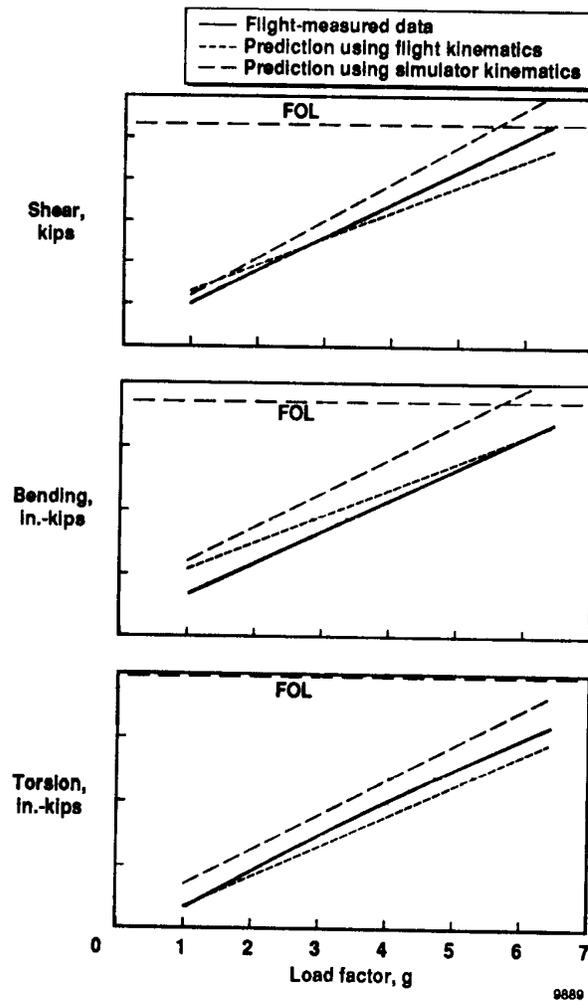
Fig. 13 Typical wing loading trends; WS 31, ACC windup turn, $M = 0.9$, $h = 10,000$ ft.

25

FOL

6.4 g

4 g

1 g

Bending,
in.-kips

0   10,000   20,000   30,000   40,000

Altitude, ft

9890
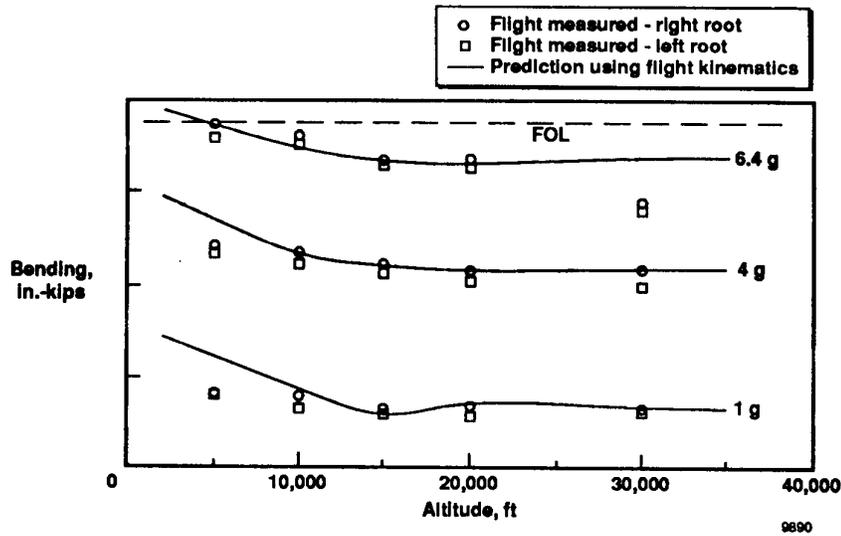
Fig. 14   Wing loading trend with altitude; WS 31, ACC windup turns, $M = 0.9$.

Region exceeding original
FOL for limit load factor

Region exceeding current
FOL for limit load factor

Extrapolated data
shown as dashes

Current FOL (100 percent proof)   6.4 g
Original FOL (80 percent proof)

5 g

Bending
in.-kips

3 g

1 g

0

Current FOL   6.4 g
Original FOL

5 g

Torsion
in.-kips   0   3 g

Original FOL (80 percent proof)   1 g

Current FOL (80 percent single hydraulic system capability)

.5   .6   .7   .8   .9   1.0   1.1   1.2

Mach

9891

Fig. 15   Canard loading trends with Mach number; ACC windup turns, $h = 10,000$ ft.
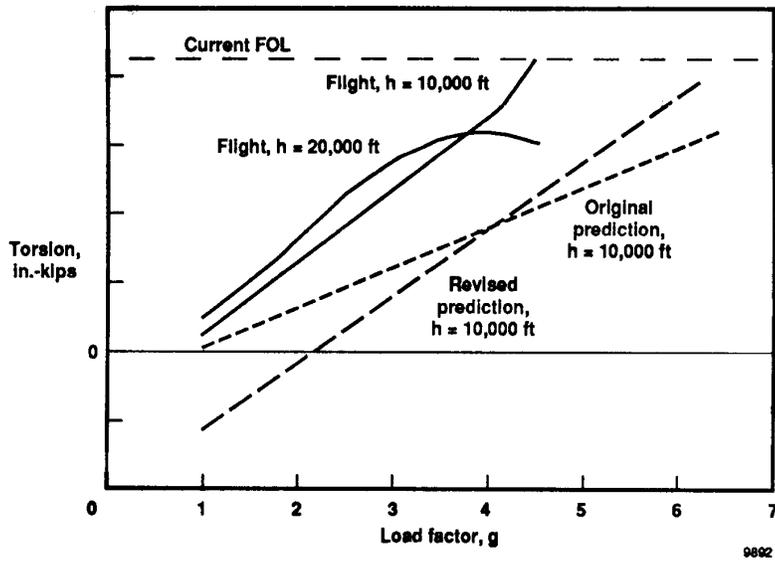
Fig. 16 Canard torsion loading trends; ACC windup turns, $M = 0.95$.
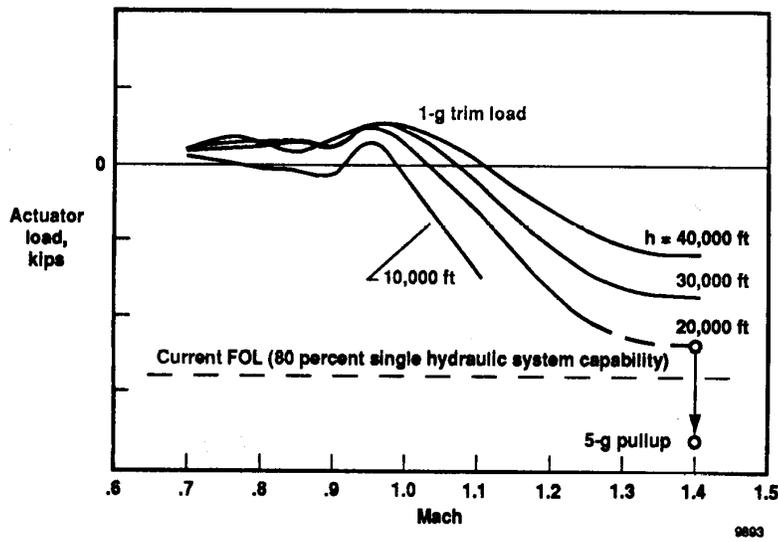
Fig. 17 Canard actuator loading trends with Mach number, ACC mode.
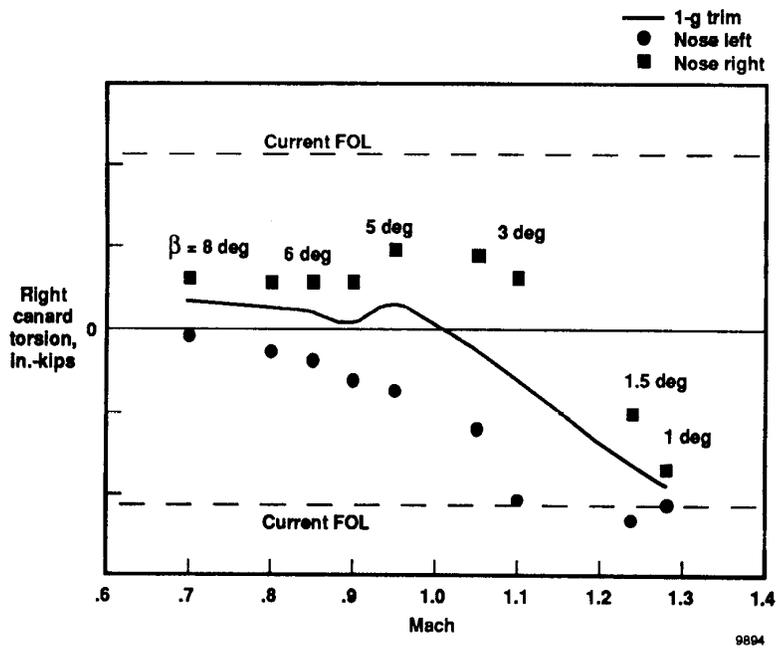
Fig. 18 Canard torsion sensitivity to sideslip; ACC full-pedal steady maneuvers, h = 20,000 ft.
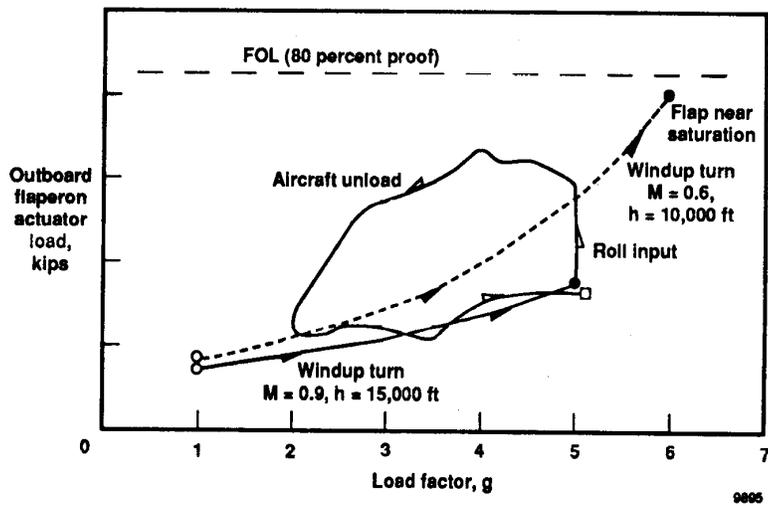
Fig. 19 Typical flaperon loading trends, ACC mode.

28
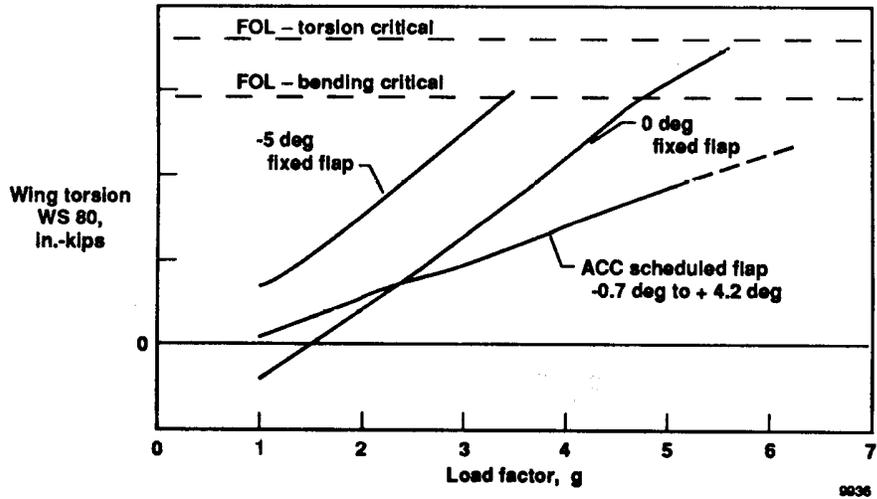
Fig. 20 Fixed versus scheduled wing flap maneuvers, windup turns; $M = 0.8$, $h = 5,000$ ft.
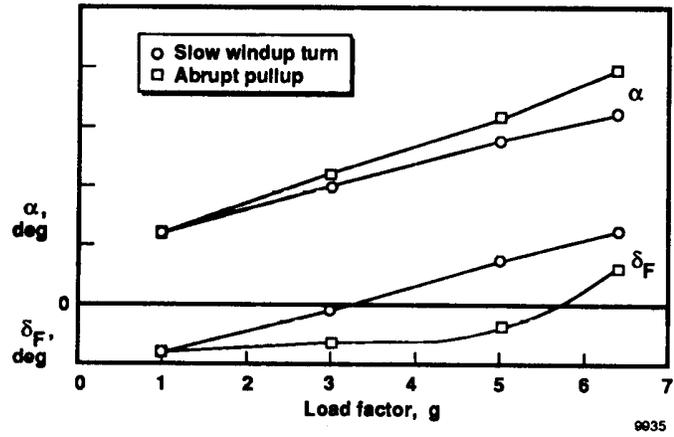

(a) Trim variables.

Fig. 21 Abrupt versus slow symmetric maneuvering; $M = 0.9$, $h = 15,000$ ft.

29
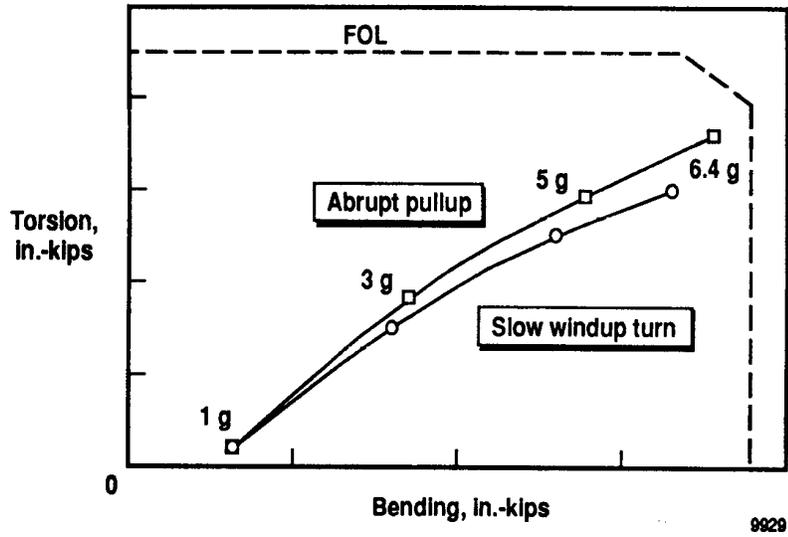
(b) Wing-root strength envelope, WS 31.

Fig. 21 Concluded.
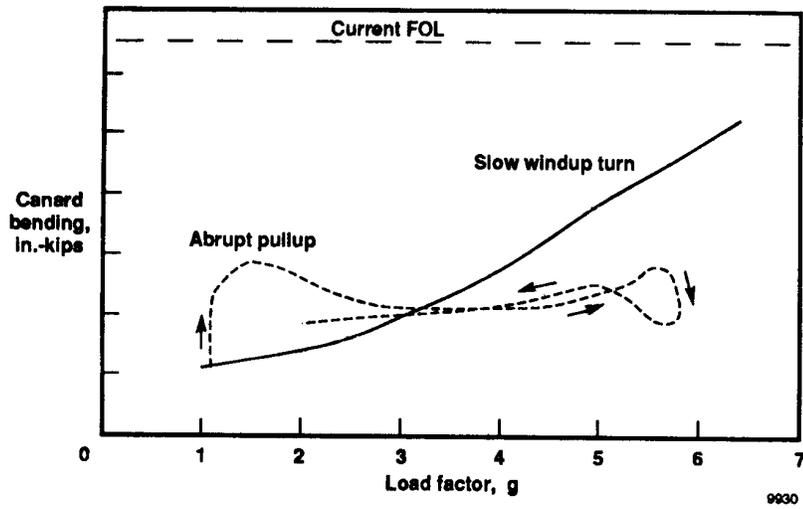
Fig. 22 Abrupt versus slow symmetric maneuvering; $M = 0.8$, $h = 15,000$ ft.
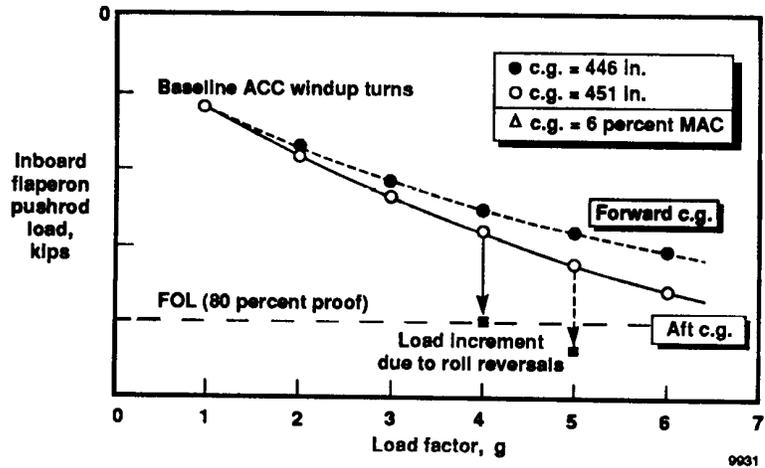
Fig. 23 Wing flaperon load sensitivity to $c.g.$ variation; $M = 0.7$, $h = 5,000$ ft.
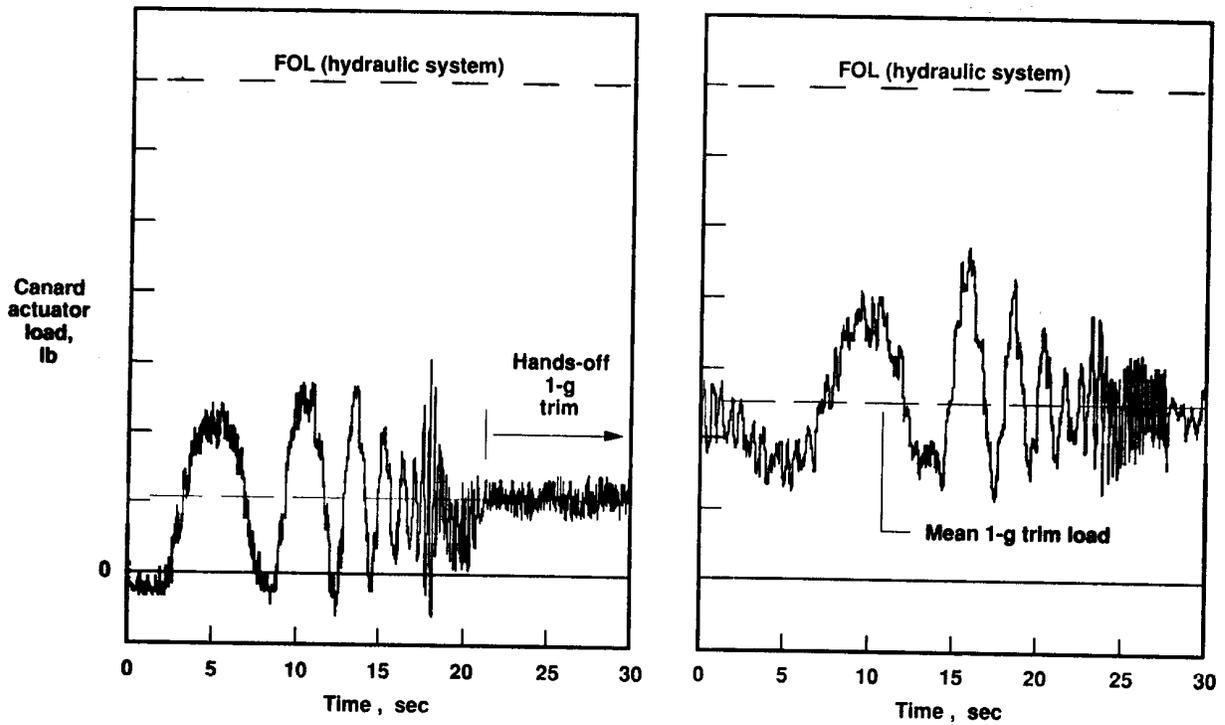
(a) Normal digital mode.

(b) Analog reversion mode.

Fig. 24 Canard actuator load comparison for longitudinal stick frequency sweeps; $M = 0.95$, $h = 15,000$ ft.

31
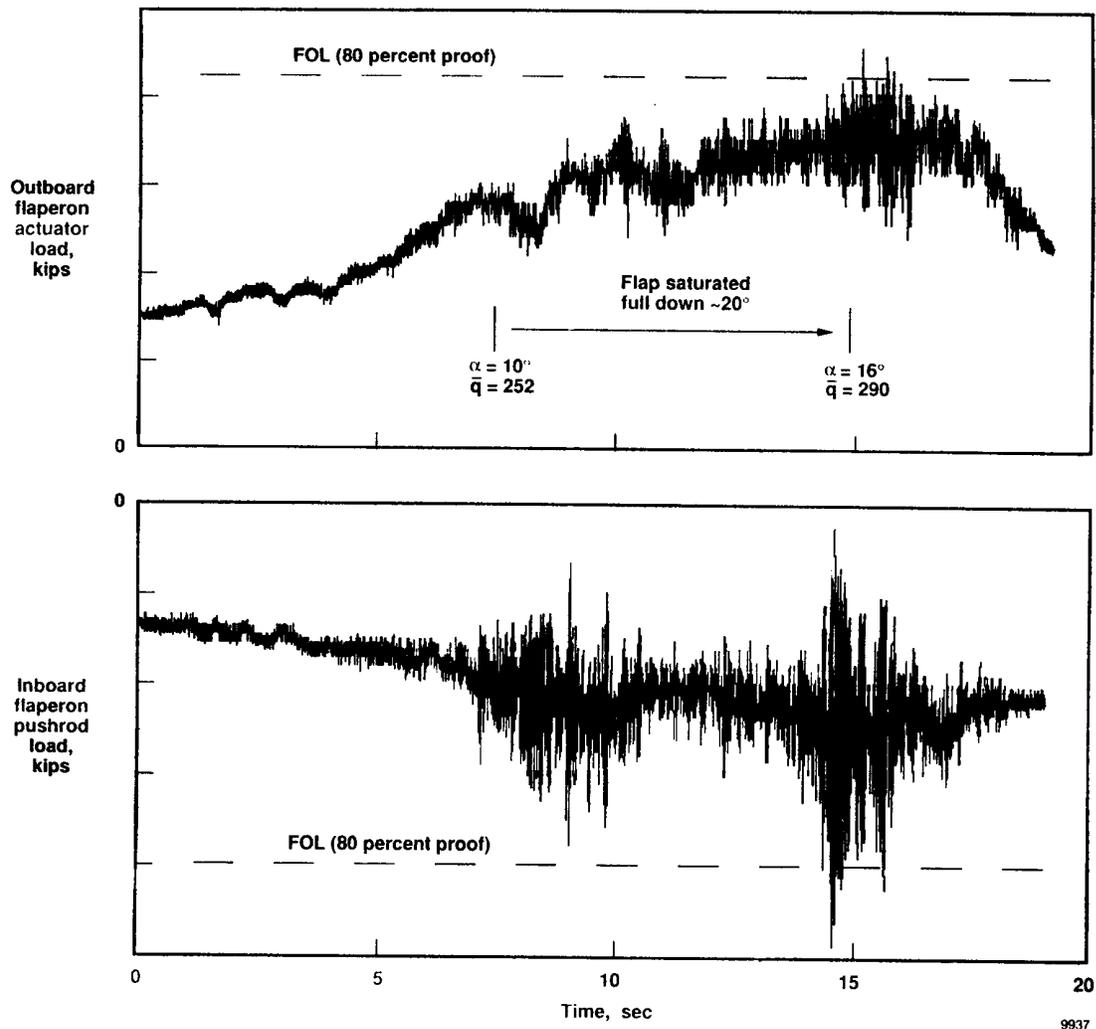
Fig. 25 Wing flaperon buffet response; ACC windup turn, $M = 0.7$, $h = 23,500$ ft.
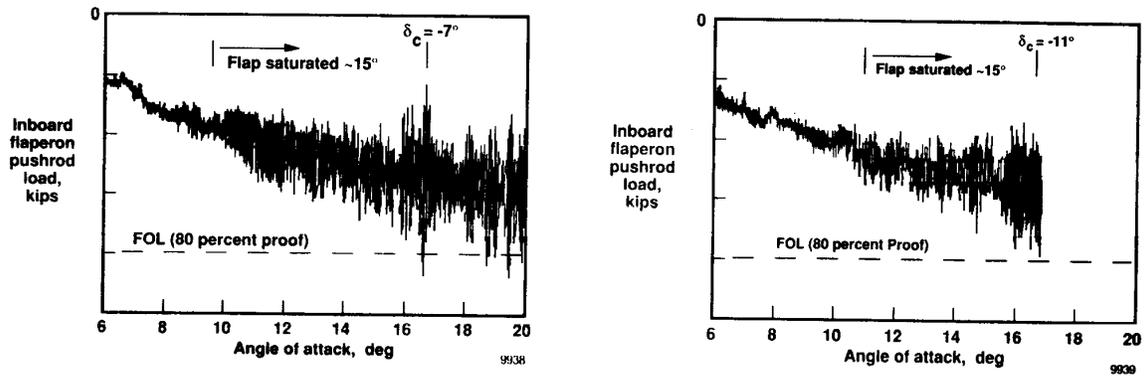
(a) Original ACC schedules.

(b) Revised ACC schedules.

Fig. 26 Effect of modified ACC schedules on wing flaperon buffet, windup turns; $M = 0.9$, $h = 35,400$ ft.
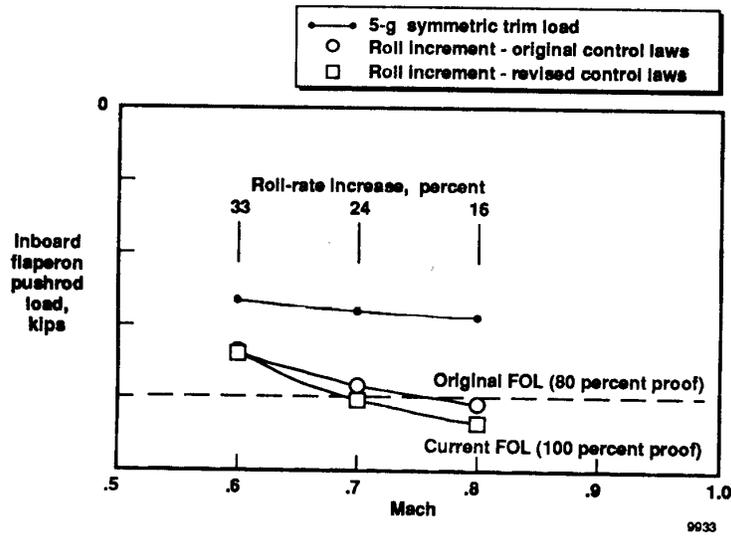

Fig. 27 Effect of increased roll agility control laws; ACC roll reversals, $h = 10,000$ ft.
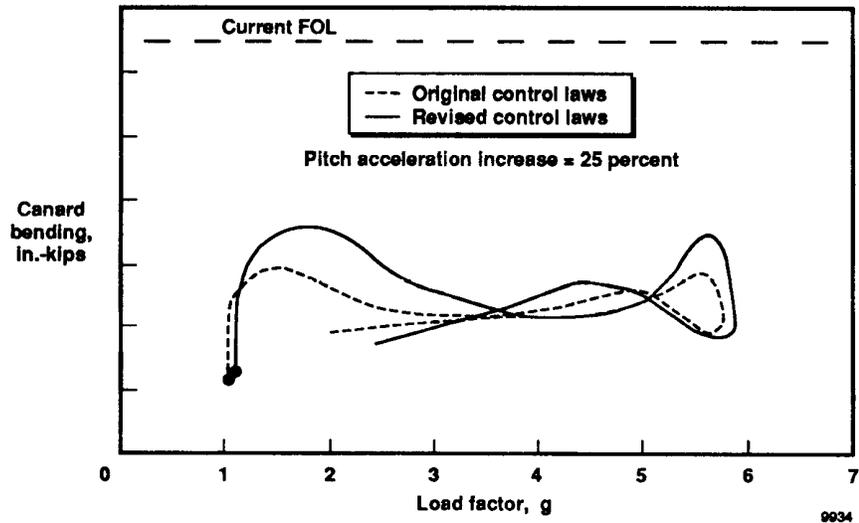
Fig. 28 Effect of increased pitch agility control laws; ACC abrupt pullups, $M = 0.8$, $h = 15,000$ ft.

Report Documentation Page

1. Report No.	2. Government Accession No.	3. Recipient's Catalog No.
NASA TM-101715		

4. Title and Subtitle	5. Report Date
X-29A Aircraft Structural Loads Flight Testing	December 1989
	6. Performing Organization Code

7. Author(s)	8. Performing Organization Report No.
Robert Sims, Paul McCrosson, Robert Ryan, and Joe Rivera	H-1574
	10. Work Unit No.

9. Performing Organization Name and Address	
NASA Ames Research Center Dryden Flight Research Facility P.O. Box 273, Edwards, California 93523-5000	RTOP 533-02-51
	11. Contract or Grant No.
	13. Type of Report and Period Covered

12. Sponsoring Agency Name and Address	
National Aeronautics and Space Administration Washington, DC 20546-3191.	Technical Memorandum
	14. Sponsoring Agency Code

15. Supplementary Notes

16. Abstract

The X-29A research and technology demonstrator aircraft has completed a highly successful multiphase flight test program. The primary research objective was to safely explore, evaluate, and validate a number of aerodynamic, structural, and flight control technologies, all highly integrated into the vehicle design. Most of these advanced technologies, particularly the forward-swept-wing planform, had a major impact on the structural design.

Throughout the flight test program, structural loads clearance was an ongoing activity to provide a safe maneuvering envelope sufficient to accomplish the research objectives. This paper presents an overview of the technologies, flight test approach, key results, and lessons learned from the structural flight loads perspective. The overall design methodology was considered validated, but a number of structural load characteristics were either not adequately predicted or totally unanticipated prior to flight test. While conventional flight testing techniques were adequate to insure flight safety, advanced analysis tools played a key role in understanding some of the structural load characteristics, and in maximizing flight test productivity.

17. Key Words (Suggested by Author(s))	18. Distribution Statement
Canards; Flight testing; Forward-swept wing; Structural loads; X-29A aircraft	Unclassified — Unlimited Subject category 05

19. Security Classif. (of this report)	20. Security Classif. (of this page)	21. No. of pages	22. Price
Unclassified	Unclassified	37	A02